Abstract

HASIB, HAZMAN BIN. Mechanical Behavior of Non-Stochastic Ti-6Al-4V Cellular Structures Produced via Electron Beam Melting (EBM). (Under the direction of Dr. Ola L. Harrysson).

Cellular metals are known for their lightweight, low volume and high surface-to-volume fraction properties, yet having good strength relative to their weight. These unique characteristics make them superior to solid metals in terms of certain applications. The rapid advancement in Additive Manufacturing (AM) technologies has virtually allowed net shape non-stochastic cellular metal structures to be fabricated with any cell shape or geometry which enables their material and properties to be tailored to meet specific requirements. Medical implants have become an important application for lattice structures. Solid prostheses are associated with issues like stress shielding and lack of tissue ingrowth. Stress shielding is the result of the mismatch in material properties between the bone and the implant, where poor stress distribution occurs at the bone-implant interface. This will cause loss of bone mass and loosening of the implant. Meanwhile, several research studies found that cellular pore sizes that are suitable for tissue ingrowth are between 50 μm to 800 μm. In this research, mechanical properties such as compressive strength and fatigue life of three different cellular structures have been investigated. The geometries examined include hexagonal, octahedral and rhombic dodecahedral. Test specimens were made of Ti-6Al-4V, fabricated via the Electron Beam Melting (EBM) process with pore sizes approximately 600 μm. Some of the specimens were chemically etched in hydrofluoric-nitric acid solution for

90 and 120 seconds to investigate the effects of etching towards mechanical properties and removal of trapped powder within the lattice structures.

Mechanical Behavior of Non-Stochastic Ti-6Al-4V Cellular Structures Produced via Electron Beam Melting (EBM)

by
Hazman Bin Hasib

A thesis submitted to the Graduate Faculty of
North Carolina State University
in partial fulfillment of the
requirements for the Degree of
Master of Science

Industrial Engineering

Raleigh, North Carolina

2011

APPROVED BY:

Dr. Ola L. A. Harrysson Committee Chair	Dr. Harvey A. West II

Professor Bryan Laffitte

Dedication

I dedicate this work to my beloved parents whose blessings have given me the strength to aim for higher and strive to excel. My special dedication goes to Sazrinah for her endless love and unconditional support.

Biography

Hazman Bin Hasib was born on March 6, 1983 in Kuala Pilah, Negeri Sembilan, Malaysia. He is the eldest of four children, with a brother and two sisters. He graduated from Sekolah Datuk Abdul Razak in 2000 and completed his pre-university education at Pusat Asasi Sains Universiti Malaya in 2002. Hazman attended Universiti Teknikal Malaysia Melaka in the same year and earned his Bachelor's degree from the Faculty of Manufacturing Engineering in 2006. In the year of 2007, he was recruited by Panasonic Compressor R&D Centre Malaysia Sdn. Bhd. as a mechanical design engineer. He served the company for 6 months before starting to work as a tutor at Universiti Teknikal Malaysia Melaka. Hazman began his master's study in Industrial Engineering at North Carolina State University in the fall of 2008 and was initiated into Alpha Pi Mu Industrial Engineering Honor Society in 2010.

Acknowledgements

I offer my heartfelt gratitude to my advisor, Dr. Ola Harrysson, who has provided me with his support in terms of patience and knowledge throughout my research and has been forthcoming with novel ideas and suggestions. He has always been a constant source of inspiration for me. I owe my accomplishment of Master's degree to his unflinching encouragement and motivation.

I extend my gratitude to Dr. Harvey West II for his willingness to serve as a member on my committee. His guidance and assistance in conducting mechanical testing are deeply appreciated. I would like to thank Professor Bryan Laffitte for agreeing to be in my committee as a minor representative and providing useful and unique insights.

My special note of thanks to my employer, Universiti Teknikal Malaysia Melaka for sponsoring my study at N.C. State University. Without their funding, it would not be possible for me to be here in the first place. My extended gratitude goes to the Dean of Faculty of Manufacturing Engineering, Dr. Mohd Rizal Salleh, for his support, patience and understanding.

I am grateful to Mr. Kyle Knowlson and Mr. Tim Horne for their prompt assistance whenever required. I also acknowledge the help and support of my friends, especially Li Yang, Gail, Li Zhang, Guha and Dinesh. Your beautiful friendship has helped me through my loneliest period of being the farthest from home.

I would like to express my sincere gratitude towards my family for their blessings and continuous support. Finally, my deepest appreciation goes to my love one, Sazrinah, for her faith and believes in me.

Table of Contents

List of Tables

List of Figures

Chapter 1 Introduction

1.1 Background

Cellular metals, also known as metal foams, can be explained as solid metals exhibiting cellular structures that form void spaces called pores. These pores take a large volume fraction of the overall structure, which leads to the high porosity characteristic of metal foams. In general, there are two broad categories of metal foams, stochastic and non-stochastic (periodic) geometries. Briefly, stochastic foams have random variations in the shape and size of the cells, where in contrast, periodic cellular structures have repeating lattice structures and can be categorized by their shapes and sizes. **Figure 1** below illustrates an example of cellular metals from each category:

Figure 1 Stochastic and non-stochastic (periodic) cellular metals.

Cellular metals have some unique characteristics that make them superior to solid metals. They are lightweight structures with low densities, but they have good strength relative to their weight. These structures also exhibit high surface-to-volume fractions. A

property or a combination of properties above makes some applications below feasible or better:

- Impact energy absorber
- Filters
- Silencers
- Heaters and heat exchangers
- Constructional materials
- Catalyst support structures
- Biomedical implants and scaffolds

Stochastic cellular metals can have either open or closed cell structures. The most common manufacturing technique to fabricate closed cell stochastic foams is by producing gas bubbles in a molten metal. This can be achieved by directly introducing gas into the melt, introducing a blowing agent to a molten metal, or through precipitation of dissolving gas in the liquid (Wadley, 2002). Open cell stochastic foams are typically made using open cell polymer foam templates, where these templates are used as a mold for the investment casting process (Ashby et al., 2000). These processes will be revisited in the next chapter, along with other manufacturing methods to produce stochastic cellular metal structures. **Figure 2** below summarizes the typical metal foam manufacturing methods (Banhart, 2000):

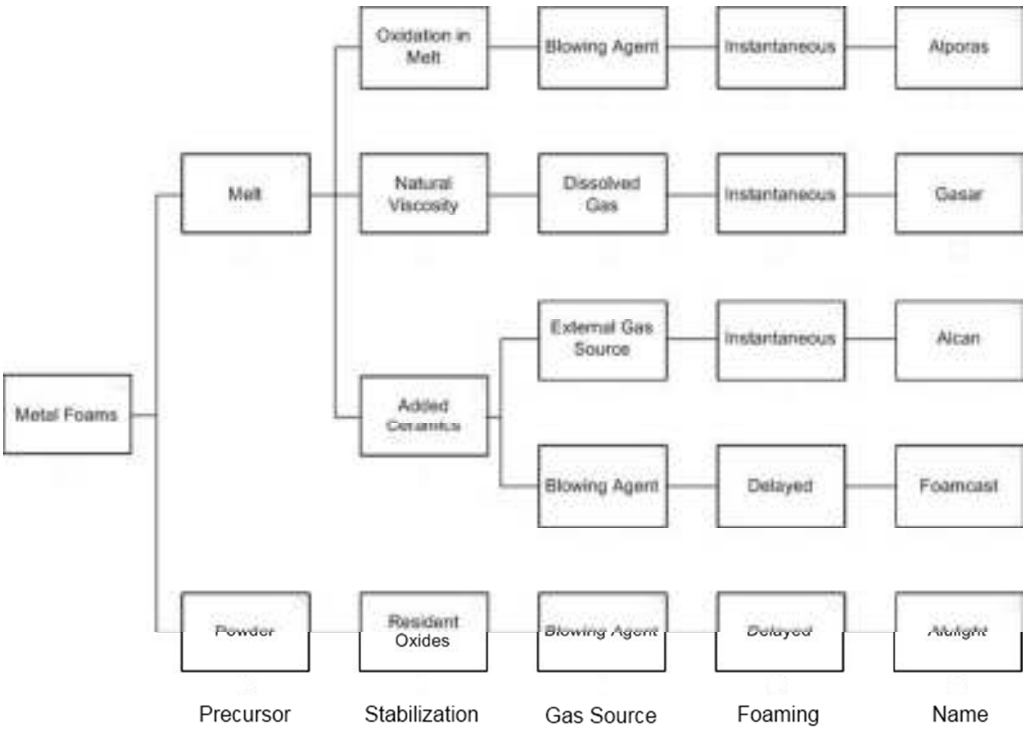

Figure 2 Classification of cellular metals manufacturing methods (Banhart, 2000).

Non-stochastic metal foams are more preferable as they do not have imperfections such as random variation of cell sizes and shapes. Furthermore, they exhibit better mechanical properties in comparison to stochastic metal foams. Conventional manufacturing of non-stochastic metal foams typically includes investment casting, deformation forming, and metal wire approaches (Wadley et al., 2003). The following classification (**Table 1**) illustrates common processes associated with stochastic and non-stochastic metal foams (Wadley, 2002):

Table 1 Manufacturing processes related to stochastic and periodic cellular metals (Wadley, 2002).

Cellular Metals		
Non-stochastic/Periodic		**Stochastic**
Lattice/Truss	**Prismatic**	
Lattice block material	Rapid prototyped	Duocel
Constructed cellular solid	Extrusions	Alporas
Tetragonal/pyramidal truss	Honeycomb	Cymat
Woven microtruss		Alulight
		Porvair
		Incofoam
		Syntactic foam
		Hollow sphere

In recent years, Additive Manufacturing (AM) technologies have evolved rapidly, and now there are several processes that focus on near net shape production of metal parts using the layer-based approach. Processes such as Electron Beam Melting (EBM), Laser Engineered Net-Shaping (LENS), and Selective Laser Melting (SLM) virtually allow net shape non-stochastic cellular metal structures to be fabricated with any cell shape or geometry. With this capability, cellular metals' materials and mechanical properties can now be tailored and optimized to design and manufacture parts to suit their requirements. For instance, biomedical implants with properties similar to that of bone can be made from

periodic cellular structures using AM techniques. Some examples of hip implants manufactured with EBM can be seen in **Figure 3** below:

Figure 3 Hip implants made by EBM process (Harrysson et al., 2008).

In EBM, parts are built by melting metal powder layer by layer. This is done by an electron beam in a high vacuum, where the kinetic energy of high speed electrons is transformed into thermal energy as they hit the powder bed. Electromagnetic fields from focusing and deflection coils are used to focus and direct the electron beam to the target. EBM can only be used for conductive materials as electrical conductivity is needed between the powder, the build plate, and the beam.

The LENS process involves direct feeding of metal powder through a deposition head to the focus point of a high powered laser beam. By doing so, the powder is simultaneously fused by the laser beam and parts are built vertically as the head moves up after successive layer. In contrast to EBM, the build plate moves in X and Y directions during the building.

The SLM process uses a strong laser to selectively melt powder material layer by layer into a mass representing a desired 3-dimensional part. The laser scans the part's cross section on the surface of the powder bed and selectively fuses the powder particles. After a layer is completed, the platform will lower and a new layer of material is applied before the process continues. SLM can be used on a wide variety of materials such as metals, polymers, ceramics, and glasses.

1.2 Research Objectives

Recently, several research projects have been conducted regarding the mechanical properties of mesh structures for biomedical implants manufactured via EBM. Harrysson et al. (2008) used EBM to manufacture Ti-6Al-4V hip implants with different mesh configurations to tailor their mechanical properties in order to reduce stress shielding. Mechanical testing such as compression testing, flexure testing and hip stem testing were conducted along with Finite Element Analysis (FEA) based on cell sizes ranging from 3mm to 12mm. However, samples with size 3mm could not be tested until failure due to the machine limitation (5000 lbs) at that time.

Similar research has been performed by Cansizoglu et al. (2008) in order to study the mechanical properties of non-stochastic structures fabricated with EBM. Hexagonal mesh cube specimens were used with pore sizes between 4mm and 6mm. The outcome of both studies show some process and design limitations and different charateristics of mechanical properties based on the load orientations and cell sizes. On the other hand, the studies did not investigate the fatigue characteristics of the structures and removal process of powder within

the cellular structure. Furthermore, the 3 mm cell size structure is not exactly in the range of optimal pore sizes for tissue ingrowth, which is between 50 to 800 μm (Harrysson et al., 2008).

The main objective of this research is to investigate the mechanical properties of non-stochastic Ti-6Al-4V cellular structures with small pores produced using EBM. This includes compression properties and fatigue characteristics. Other objectives are to study the effects of different cell geometries, particularly hexagon, octahedron, and rhombic-dodecahedron cells, and also study the effects of chemical etching towards mechanical properties, surface roughness conditions for tissue ingrowth, and the removal of trapped powder within the structure. The final objective is to validate the experimental results with FEA analysis.

Chapter 2 Literature Review

Chapter 1 of this thesis provided a brief introduction to cellular structures, including their applications, classifications (stochastic and periodic), and conventional manufacturing techniques. Furthermore, due to the emergence of Additive Manufacturing (AM) technologies, cellular structures' materials and mechanical properties can now be tailored and optimized to design and manufacture parts to suit their requirements, and several AM techniques such as EBM, SLS, and LENS can be used for this purpose. This chapter reviews fabrication methods of cellular structures, Electron Beam Melting (EBM) technologies, and previous research on the mechanical properties, and concludes with a statement of the research problem.

2.1 Cellular structures fabrications

2.1.1 Stochastic foams

Various manufacturing methods to build stochastic foams have been discussed, either for the closed or open cell structures, such as Davies and Zhen (1983), Ashby et al. (2000), Banhart (2000), and Wadley (2002). The earliest attempt of making metal foams was in the 1940's by Benjamin Sosnick, where he tried to foam aluminum using the vaporization of mercury. From this idea, William Elliot successfully produced foamed aluminum by introducing a blowing agent to a molten metal and heating the mixture to evolve gas as the heat decomposes the blowing agent (Davies and Zhen, 1983; Banhart and Weaire, 2002).

The decomposition process forms bubbles which create voids in the melt, and a foamed solid is obtained after the melt is cooled.

This method is still being used for closed cell cellular structure fabrication, where titanium hydride (TiH_2) is widely used as the foaming agent. Aluminum is melted and the temperature is stabilized around 690˚C before calcium is added to increase the melt viscosity. After being stirred, titanium hydride is added into the melt and bubbles are created due to rapid forming of hydrogen gas as the titanium hydride decomposes into Ti and H_2 gas. This method produces metal foams with cell sizes ranging from 0.5 to 5 mm and relative densities from 0.2 to 0.07 (Ashby et al., 2000). In addition, there are other ways to generate gas bubbles in a molten metal. Gas can either be introduced directly into the molten pool or precipitated from previously dissolved gas in the molten metal, which is known as the Solid-Gas Eutectic Solidification (Banhart, 2000).

The method of introducing gas directly into the melt consists of two steps, preparation of a metal-matrix composite (MMC) melt and foaming of melt by injecting gases such as nitrogen, air or argon into it (**Figure 4**). The foams are uniformly distributed from the action of a stirring paddle or rotating impellers. Typical foams produced with this method are NORSK-HYDRO and CYMAT, having cell pores with diameters between 5 and 20mm, and relative densities between 0.1 and 0.03 (Ashby et al., 2000). Solid-Gas Eutectic Solidification method works on the principle that a eutectic condition is formed between hydrogen gas and numerous liquid metals. An alloy is melted in a furnace under an appropriate pressure and later poured into a mold. Eutectic solidification occurs during the pouring, resulting in a large volume fraction of pores. Materials produced this way are

known as GASAR (illustrated in **Figure 5**), and they exhibit pore diameters ranging from 0.01 to 10 mm and porosities ranging between 0.05 and 0.75 (Banhart, 2000). Apart from using gas bubbles to create closed cell foams, alternative methods to build closed cell foams include sintering of hollow spheres, controlled dissolution of gas (Ashby et al., 2000), and foaming of compacted metal powder (Banhart, 2000).

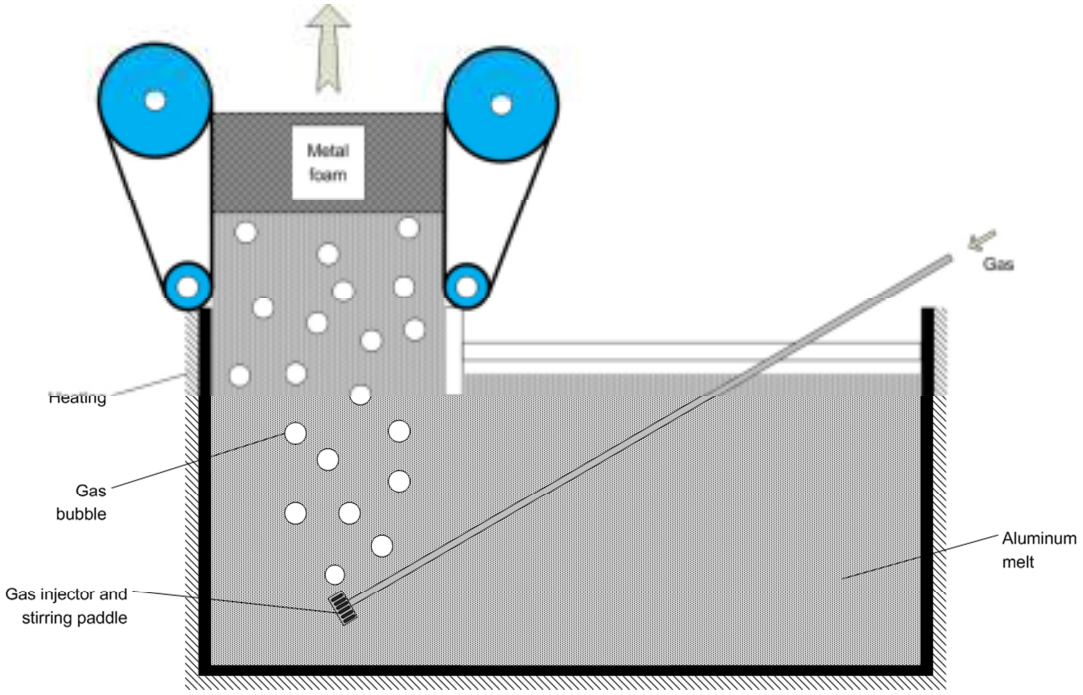

Figure 4 Gas injection into the melt (Wadley, 2002).

Figure 5 Illustration of GASAR foam (Ashby et al., 2000).

In a recent development, Rabiei and Vendra (2008) produced closed cell composite foams with powder metallurgy (PM) and casting methods. Solid matrix material from casting and powder metallurgy is used to fill the vacancies around preformed hollow spheres, where in PM techniques, hollow spheres and matrix powder are vibrated before undergoing the sintering process. In the casting method, spheres and matrix material are also vibrated to set them into a random loose arrangement and then cast into a mold after being preheated at 700˚C. The resulting compressive strengths are 127 MPa for PM foams and 105 MPa for cast foams, which are significantly higher than similar foams compared in this study, developed by Fraunhofer Institute and Georgia Tech (23 MPa and 5 MPa respectively).

Open cell stochastic foams are typically made using open cell polymer foam templates, where these templates are used as a mold for the investment casting process (Ashby et al., 2000). A mold template is selected, coated with a ceramic slurry, and baked to obtain the negative image of the foam. The mold material is then removed after the liquid metal is cooled and solidified. Foams fabricated via this process are known as DUOCEL.

Polymer templates can also be used as a substrate for chemical vapor deposition (CVD), a method typically used to create open cell nickel foams (INCOFOAM). A nickel carbonyl precursor is used to coat exposed surfaces of the templates in a heated reactor (at 120˚C). Foams are completed after the template is removed by heating in air and the resulting metal ligaments are sintered. Other processes that are related to open cell foam manufacturing are solidification of liquid metal and powder coating technologies.

Another process used to create open cell foams is self-propagating high-temperature synthesis (SHS), also known as combustion synthesis (CS). In this process, a compacted powder mixture is ignited in either air or an inert atmosphere. With sufficient heat released from the ignition, the mixture will produce a self-sustaining chemical reaction, also known as an exothermic self-propagating reaction (Ryan et al. 2006). The stages involved are shown in **Figure 6**. Porous structures of NiTi shape memory alloy have been fabricated using this process (Chu et al., 2004), where good mechanical properties were obtained with a compressive strength of 208 MPa, and an elastic modulus of 2.26 GPa which is close to that of the cancellous bone (0.1-1.5 GPa).

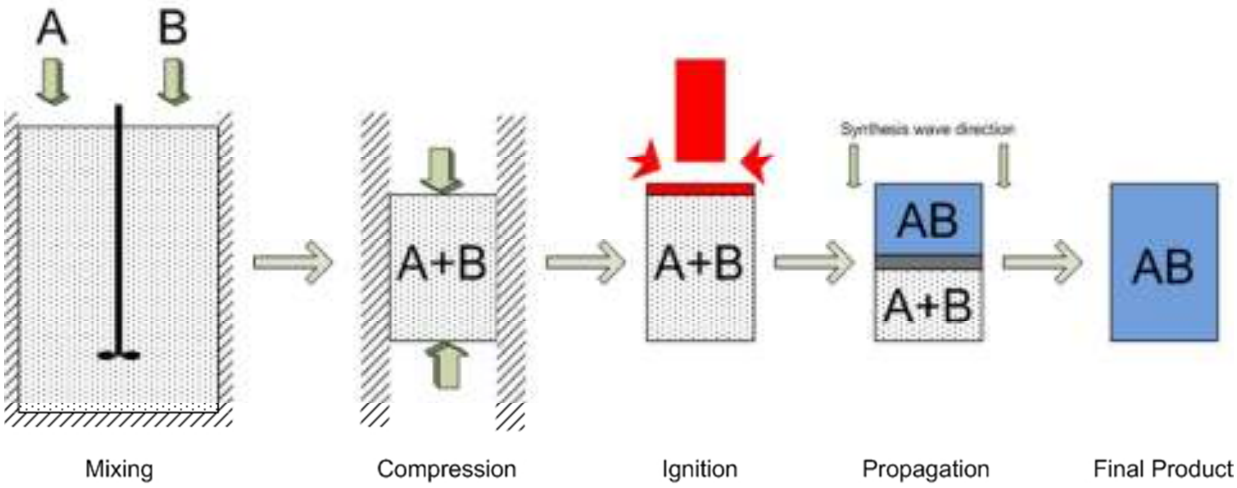

Figure 6 Schematic representation of the stages involved in combustion synthesis (Ryan et al., 2006).

2.1.2 Non-stochastic foams

Stochastic cellular structures have several imperfections that might affect their mechanical properties. Among those imperfections are cell size and shape variations, missing cells, cell wall waviness, and cell wall misalignment. Localized deformations based on loading conditions could occur due to these deficiencies which will affect the strength and stiffness of the structures (Chen et al., 1999; Grenestedt, 2005). This is supported by several studies which reported that non-stochastic cellular structures are superior for structural applications as they can sustain loads at weights better than stochastic foams (Wadley, 2002; Wadley et al., 2003; Queheillalt and Wadley, 2005).

Wadley et al. (2003) and Wadley (2002) discussed several manufacturing methods of non-stochastic cellular structures. One of them is investment casting. Truss core patterns made from polymer are either rapid prototyped or injection molded, and coated with a ceramic slurry. A mold is created upon removal of the polymer through melting and the mold

will be filled with liquid metal. Another method that was discussed in the studies is deformation metal wire weaving. Sandwich panels constructed with structures made from a metal wire weaving process have been found to have stiffness similar to honeycomb structures. In a recent study by Queheillalt (2009), Ti-6Al-4V sandwich structures were made using a high-temperature forming and diffusion bonding method. A single layer lattice truss core is made by perforating a sheet to create a pattern followed by cold bending at the nodes. Then the face sheets are attached to the core by hot forming or diffusion bonding processes. The highest compressive peak strength achieved from the structure is found to be around 10 MPa.

In relation to the biomedical area, Kusakabe et al. (2004) produced a hip implant with a mesh surface stem from Ti-6Al-4V. The mesh structure is obtained by stacking layers of patterned plates made by a chemical etching process. The layers are bonded together through a diffusion and evaporation-condensation process at 900˚C. The structure was reported to have pore sizes in the range of 500 to 1000 μm with 80% porosity.

2.1.3 Non-stochastic cellular structures via Additive Manufacturing

2.1.3.1 Direct Laser Forming (DLF)

The DLF technique (also known as Selective Laser Melting) utilizes a strong laser to fuse metal powders into a mass. A layer of powder is spread uniformly over the build platform with a wiper mechanism before it is fully melted by a high density laser according to the geometry of the part cross section. The melted particles will then fuse and solidify to produce a layer of the part cross section. The fabrication platform is lowered by a layer thickness, new powder is delivered, and the process repeats until the build is completed. The

whole process takes place in a build chamber in an inert environment, where Argon or Nitrogen gas is usually used. The schematic configuration of a DLF process is shown in **Figure 7** below:

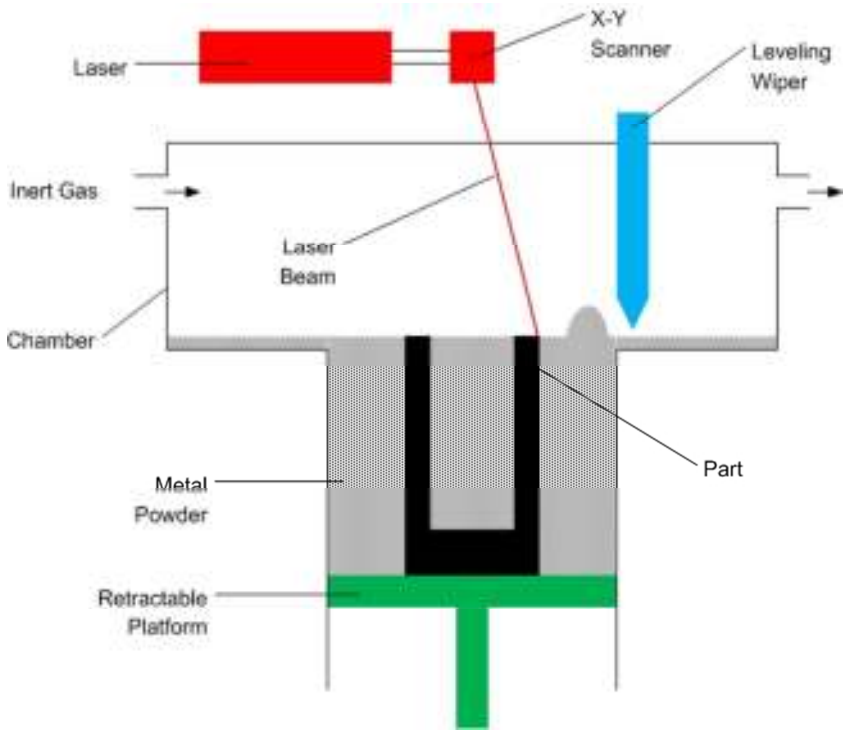

Figure 7 Schematic configuration of DLF process.

Hollander et al. (2006) used the DLF process to study the effect of porosity in an in-vitro environment. Porous discs with a cubic pore pattern were built from Ti-6Al-4V powder particles, with nominal pore diameters of 1000, 700, and 500 μm. The discs were cleaned with sand-blasting and the actual pore diameters measured with SEM were approximately 700, 400, and 200 μm respectively. Human osteoblasts were cultured on the disc for the periods of 3, 7 and 14 days, where a standard cell culture plastic was used as a control. The

evaluation after 14 days revealed that the disc with 200 μm had more cells grown over the surfaces compared to the other two.

2.1.3.2 3D Fiber Deposition

This particular method operates on an extrusion principle. Li et al. (2006) fabricated a porous Ti-6Al-4V scaffold via this process. Titanium slurry required for extrusion was prepared by mixing Ti-6Al-4V powder with methylcellulose and stearic acid. The slurry is placed in a syringe and deposited through a nozzle under pressure. The extrusion path is controlled by a positional control unit connected to a computer. Finally, the part needs to be sintered in a high vacuum furnace at a temperature up to 1250˚C. Depending on pressure and feeding speed applied, the maximum porosity of around 74% was achieved. The feeding speed was also proven to affect the compressive strength of the structure.

2.1.3.3 Direct Metal Laser Sintering (DMLS)

Direct Metal Laser Sintering (DMLS) was developed by EOS GmbH. Similar to SLM, DMLS is also a laser-based process. DMLS can produce a part with 95% density relative to original material. In this process, metal powders are completely melted by the scanning of a high power laser beam. The process is as illustrated in **Figure 8**. The powder dispenser piston raises the powder supply and then a recoater arm distributes a layer of powder onto the powder bed. A laser then melts the layer of powder particles. After a layer is built, the build piston lowers the build platform and the next layer of powder is applied, and the process is repeated until the build is finished.

In a research study done by Bertol et al. (2010), a mandible implant with porous internal structures was fabricated via DMLS. The implant was built on a model EOSINT

250X machine from Ti-6Al-4V powder, with a layer thickness of 50 µm. The researchers used a spherical structure provided by the software package as the internal structure (the pore size of the structure is not mentioned in the literature). Finally the implant was digitally scanned and compared to the CAD model. The reported difference in the majority of the areas was not over 50 µm.

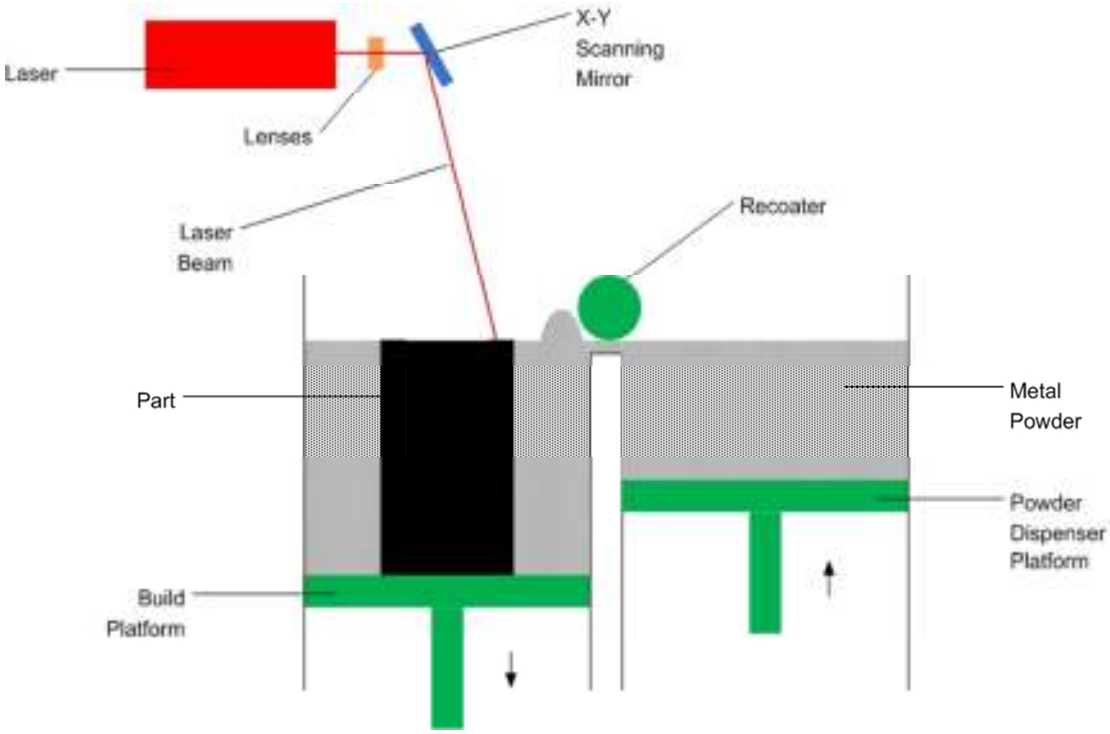

Figure 8 Direct Metal Laser Sintering (DMLS).

2.1.3.4 Laser Engineered Net Shaping (LENS)

This process was initially developed by Sandia National Laboratory and has been commercialized by OPTOMEC. The metal powder is melted by a high power laser, typically in the range of 500 to 1000W. Unlike SLM and DMLS, the same head is used to deliver the powder and the laser beam coaxially, as shown in **Figure 9**. An inert gas which is often used

to shield the melt pool from atmospheric oxygen is also supplied through the same head. The build platform does not move during the build, but instead, the head moves in the Z direction until the part is completed. This characteristic makes the LENS process very useful for repair operations.

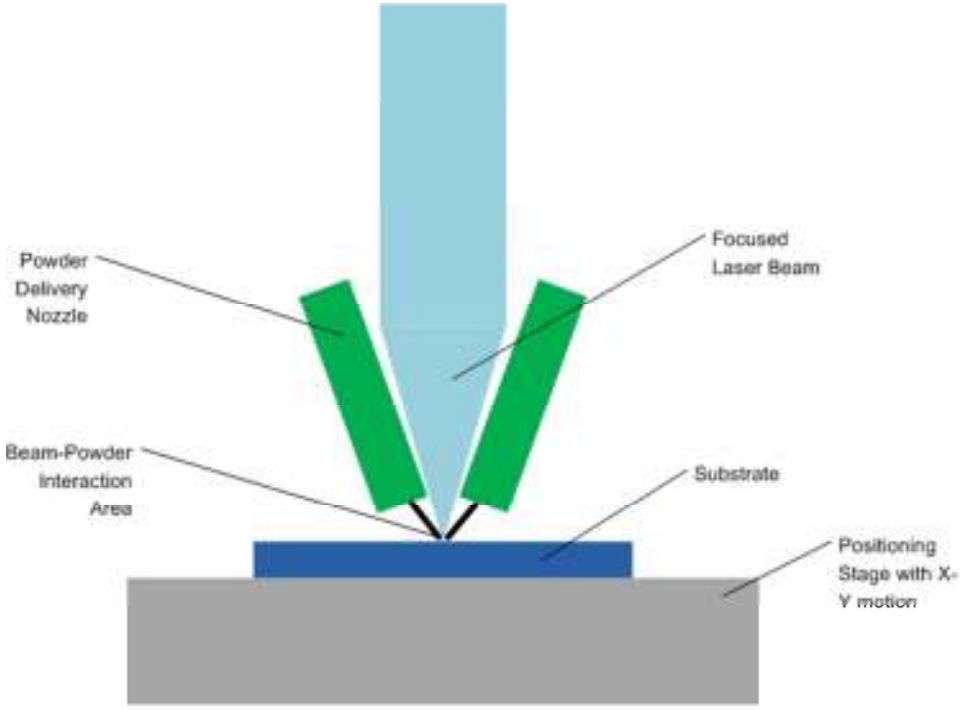

Figure 9 Laser Engineered Net Shaping (LENS).

A study on mechanical properties and in vitro biocompatibility of porous CoCrMo alloy structures fabricated via LENS has been undertaken by Espana et al. (2010). Different values of parameters (scan speed, powder feed rate and laser power) were used to study their influence towards the structure's properties. The samples were built in a manner where they had a porous core with a fully dense outer surface. The relative density obtained varied from 0.81 to 0.90 while the Young's modulus of the samples were reported to be between 33 GPa

and 43 GPa. In addition, the average compressive strength measured was between 948 MPa and 1943 MPa.

2.1.3.5 Electron Beam Melting (EBM)

Arcam, a company founded in Sweden, is responsible for developing and commercializing the Electron Beam Melting (EBM) technology. The current commercial models are A1 and A2, where A1 is the latest model produced by Arcam, specifically designed for implant manufacturing. The EBM process is capable of building fully dense metal parts. A powerful electron beam (0.5 to 3.5 kW) is used to build up parts layer by layer by the melting of metal powder, according to the exact geometry from the 3-dimensional CAD model. The CAD model is previously sliced into thin 2D layers using special software, typically 0.1 mm or 0.07 mm in thickness.

The EBM process works based on the electrons' kinetic energy principal. The emitted electrons from the filament accelerate at a very high speed towards the build substrate, creating an electron beam. When these electrons collide with the metal powder, heat is produced as the electrons' speed is reduced and the kinetic energy converts into thermal energy, and this heat melts the powder particles. The electron beam is generated within the electron beam gun, consisting of an anode, a cathode and electromagnetic focusing and deflection units.

In this gun, the tungsten filament (cathode) is heated up and emits electrons when an electrical current is passed through it. Meanwhile, a 60,000 V current is applied to the anode beneath the filament and this very high potential voltage difference helps to accelerate the electrons from the filament in the desired direction. The resulting beam is then focused

electromagnetically by a focusing coil. After that, the beam will pass another electromagnetic coil (known as the deflection coil) where it is deflected on specific areas onto the build plate at a scanning speed as high as 4000 m/s. This very high scanning speed is achievable due to the MultiBeam technology introduced in the current software, EBM Control 3.2. The previous scanning speed was reported to be only as high as 1000 m/s (Cansizoglu, 2008).

An astigmatism coil assists to keep the beam in focus regardless of its position on the build plate. Without this coil, the focus point of the beam tends to have a wider area (elliptical shape) when it is deflected towards the edge of the build region. The entire process is executed under vacuum. This vacuum environment prevents the collisions of electron particles with gas atoms which can lead to scattering of the electron beam. In addition, the build chamber is made from thick stainless steel with a dual layer glass on the viewing panel for two main purposes, maintaining vacuum pressure and blocking radiation. Radiation existing as x-rays is emitted when the electrons hit the powder particles. **Figure 10** shows the major elements of the Electron Beam Melting process described above.

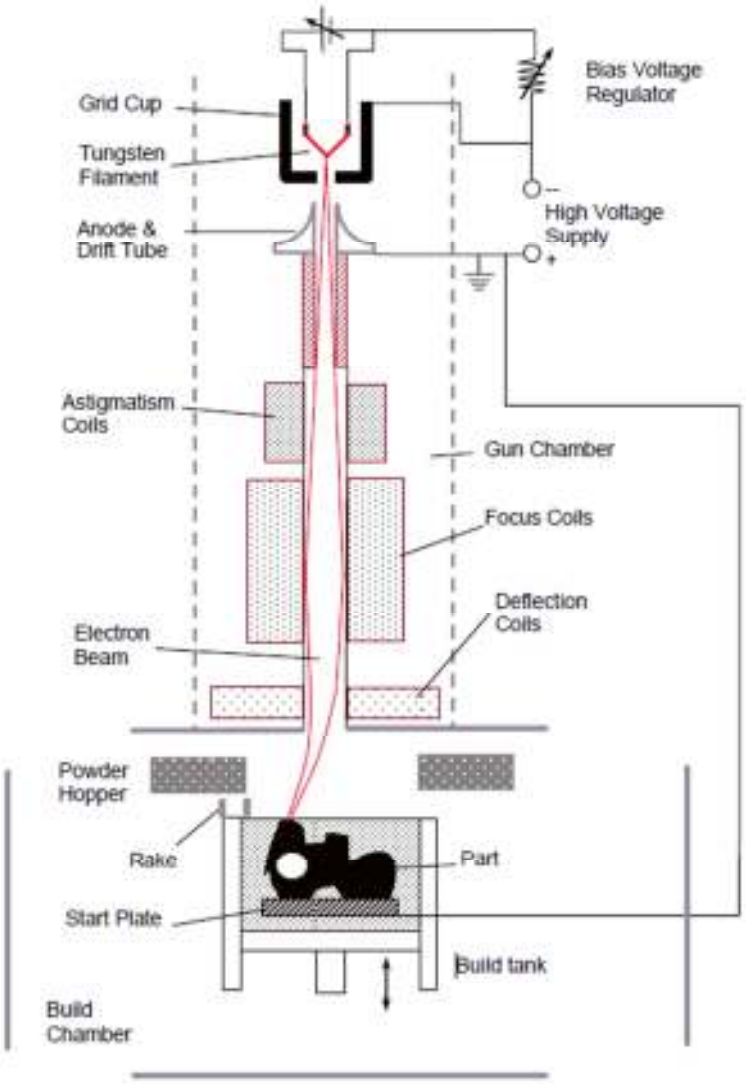

Figure 10 Explanatory sketch of Electron Beam Melting (EBM).

Similar to other processes such as DMLS and SLM described above, the powder particles are melted layer by layer according to the predetermined thickness. However, in between the layer melting processes, the metal powder is preheated. This is important to keep the part being built at an elevated temperature which will lead to the reduction of thermal stresses within the part (Cormier et al., 2004). In addition, the preheating process also

provides some initial sintering between the new layer of powder and the previously melted layer which is critical as it increases thermal and electrical conductivity (Cansizoglu, 2008).

In comparison to laser-based SFF systems, EBM has several advantages. Energy from the electron beam is fully utilized, providing high power efficiency. Laser-based systems are associated with reflectivity problems, where some portions of the beam are reflected when the beam hits shiny powder surfaces, thus reducing efficiency. Oxidation is also prevented in EBM as the metal melting process is done in a vacuum environment. On the other hand, a process such as the SLM requires the sintering process to be done in an inert gas surrounding. In a study done by Harrysson et al. (2009), EBM and DMLS techniques were compared in terms of medical implant fabrication. It was found that EBM produced the same parts in shorter time, but due to relatively poor surface roughness and details obtained, further machining processes might be required, and this will affect overall cost of the fabrication. The research has concluded that EBM is significantly more economical for large implants without small features, as the time it takes to be produced in DMLS is far too long.

The EBM has been used to manufacture cellular structures for various purposes. Kumar (2009) studied the relationship between cell geometries (shape and density) and electrical conductivity in Ti-6Al-4V lattice structures, while Manogharan (2009) optimized hexagon and rhombic dodecahedron cell designs to increase efficiency in heat transfer applications. In another study by Schwerdtfeger et al. (2009), Ti-6Al-4V cellular structures with negative Poisson's ratio (auxetic structures) were built with the Arcam A2 and their mechanical properties were studied. The EBM is also widely used in the biomedical area. Springer (2010) built titanium alloy scaffolds with different surface characteristics for in

vitro experiments of human tissues. One of the designs includes a porous structure with pore sizes around 650 μm. Meshed implants have also recently been fabricated using the EBM system. Harrysson et al. (2008) manufactured hip implants with customized mechanical properties to reduce stress shielding and bone remodeling. A prototype of a tibial knee stem has also been built by Murr et al. (2009) (**Figure 11**) and its build structures and microstructures have been observed.

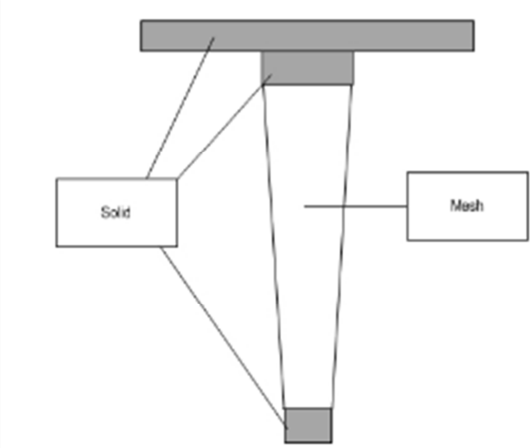

Figure 11 Illustration of tibial knee stem made by Murr et al. (2009)

2.2 Properties of metallic foams

2.2.1 Structural characteristics

2.2.1.1 Relative Density

Gibson and Ashby (1997) indicated that relative density is the most important structural feature for metallic foams. In general, relative density is the proportion of the foam's density compared to the density of the solid which the foam is made of, which can be calculated by ρ/ρ_s (where ρ is the density of the foam and ρ_s is the density of the solid). The

porosity of a cellular structure is simply (1 - ρ/ρ_s) and can be defined as the volume fraction occupied by the pore space in the structure. Ashby (2006) and Wadley (2006) suggested that the relative density in a structure can be manipulated by modifying cell's edge length and wall thickness. Both literatures provided some mathematical equations on calculating relative density for certain cell geometries in relation to their edge length and wall thickness.

Cansizoglu et al. (2008) studied compressive properties of titanium cellular structures with hexagonal pores made by EBM. It is reported that the modulus and compressive strength were increased by the incremental change in relative density. The structures were built with the same strut and cube size, but with different cell spacing that varied the relative density of the overall structure.

2.2.1.2 Cell topology and shape

Cell topology can be either closed or open cells. Closed cells have membrane-like surfaces which seal them off from the neighboring cells. On the other hand, open cells do not have this criterion which allows them to be interconnected with each other (Gibson and Ashby, 1997). Besides topology, cell shape also plays an important role in contributing to the structure's properties. In three dimensional arrays, various cell shapes can be packed together to fill space and build up a non-stochastic cellular structure. **Figure 12** shows several shapes of unit cells while **Table 2** summarizes the properties of unit cell geometries commonly considered for cellular structures (where *h* is the height of the unit cell and *l* is the length of the strut).

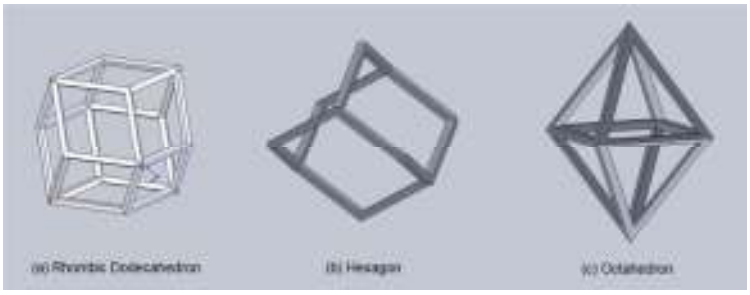

Figure 12 Examples of commonly used unit cells.

Table 2 Geometric properties of unit cells (Gibson and Ashby, 1997).

Cell Shape	Cell volume	Surface area	Edge length
Tetrahedron	$0.118l^3$	$3l^2$	$6l$
Triangular prism	$0.433lh^2$	$0.86l^2+3lh$	$6l+3h$
Square prism	lh^2	$2l^2+4lh$	$8l+4h$
Hexagonal prism	$2.598lh^2$	$3l^2+6lh$	$12l+6h$
Octahedron	$0.471l^3$	$3.46l^2$	$12l$
Rhombic Dodecahedron	$2.79l^3$	$10.58l^2$	$24l$

2.2.2 Mechanical characteristics

In general, the mechanical properties of metallic foams have very little dependency on the absolute cell size (Gibson and Ashby, 1997). However, it is mentioned that cell topology (open or closed) affects the linear elasticity mechanism of the structure. In closed cell foams, the edges of the cells are subjected to bending and extending motions, and their modulus of elasticity will also include the stretching of the outside membranes. The elastic modulus for closed cell foams is given as:

$$\frac{E_{foam}}{E_{solid}} = C_1\left(\frac{\rho_{foam}}{\rho_{solid}}\right)^2 + C_2\left(\frac{\rho_{foam}}{\rho_{solid}}\right) \tag{1}$$

where E is the modulus of elasticity, ρ is the density, while C_1 and C_2 are the proportionality constants. Open cell foams have a simpler model as the deformation occurs in terms of strut or truss bending. Equation 2 below describes the modulus for open cell structures:

$$\frac{E_{foam}}{E_{solid}} = C_3\left(\frac{\rho_{foam}}{\rho_{solid}}\right)^2 \tag{2}$$

Similarly, Ashby et al. (2000) provided a scaling relation for the compressive strength of open cell foams as below:

$$\frac{\sigma_{foam}}{\sigma_{solid}} = C_4\left(\frac{\rho_{foam}}{\rho_{solid}}\right)^{\frac{3}{2}} \tag{3}$$

where the constant C_4 has value within the range of 0.1 to 1.0. Ashby (2006) also characterized non-stochastic cellular structures' mechanical properties based on two different features known as bending dominated structures and stretch dominated structures. This classification is made based on Maxwell's stability criterion, which is later generalized by Calladine (1983) for three dimensional arrays as:

$$M = b - 3j + 6 = s - m \tag{4}$$

where b is the number of struts and j is the number of nodes, while s and m are the numbers of states of self-stress and of mechanism. From this equation, bending dominated structures will have the values of $M<0$ and stretch dominated structures will have $M\geq 0$.

Cellular structures can have bending dominated behaviors regardless of their topology, open or closed cell. In fact, any polyhedral with space filling properties will not exhibit $M\geq 0$ (Ashby, 2006). Some examples of space filling polyhedrals are triangular prism, rectangular prism, hexagonal prism, rhombic dodecahedron and tetrakaidecahedron (Gibson and Ashby, 1997). Bending dominated structures have similar properties as metallic foams as shown in **Figure 13**. One of the advantages of these structures is their energy absorbing capability which is indicated by the plateau stress in the curve.

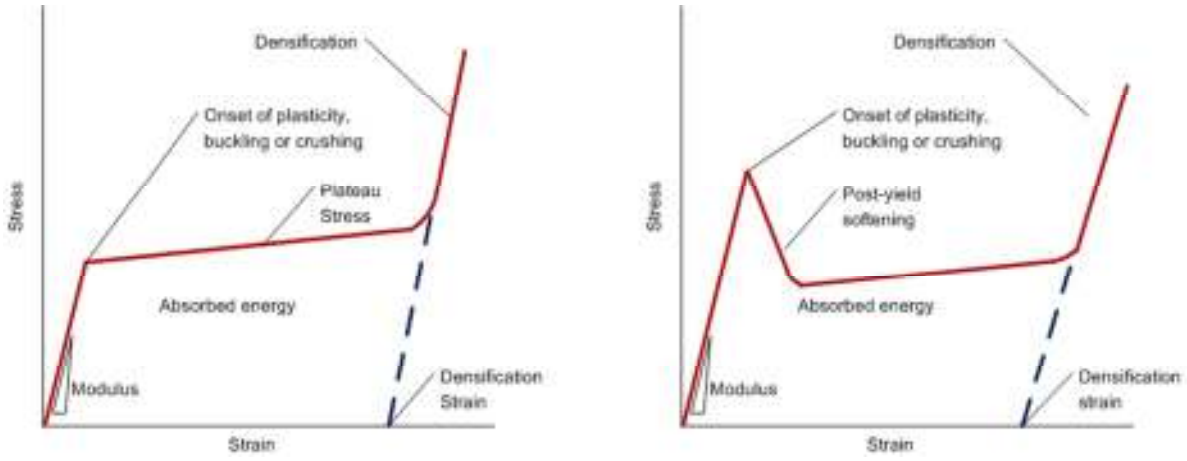

Figure 13 Stress-strain curve for bending dominated structure (left) and stretch dominated structure (right).

Stretch dominated structures can be obtained by combining two or more non-space filling polyhedrals with $M\geq 0$ to create a space filling structure. For instance, a combination of octahedron and tetrahedron satisfies this condition. As can be seen from **Figure 13**, the

stress-strain curve produced by these structures is somewhat different from the bending dominated structures.

Comparing both types of structures having the same relative density, the stretch dominated structures will show significantly higher modulus and yield strength (Ashby, 2006). This behavior makes them very suitable candidates for lightweight structural applications. In contrast, they suffer from a post-yield softening condition due to brittle struts failing which hampers their ability to absorb much energy.

Figure 13 also shows a densification stage when cellular structures are compressed. However, Cansizoglu (2008) reported that no densification occurred when the compression test was conducted for his structure. This is caused by the continuity of bending and buckling of the struts as the movement of other node points was not limited by the absence of limiting connections. Cansizoglu also stated a process limitation for building cellular structures via EBM. The limitation is illustrated in **Figure 14** below, where structures with their struts built at angle below 20˚ with respect to the build plane showed poor structural integrity due to very small overlaps between adjacent layers.

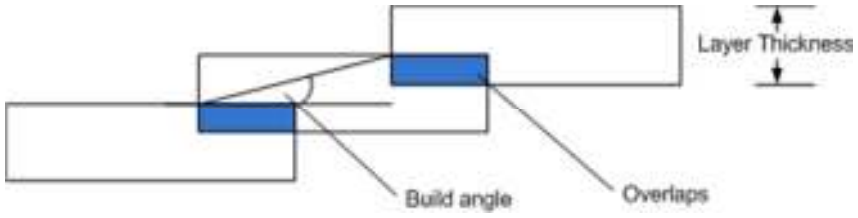

Figure 14 Overlaps between adjacent layers.

2.2.2.1 Finite Element Analysis (FEA) of cellular structures

Periodic cellular materials exhibit symmetrical properties which allow the stress, strain and displacement of the structures to be mapped from a unit cell in FEA. The symmetries present in these structures also permit the derivation of the boundary conditions of the unit cell without using any simplifications or assumptions (Kim and Al-Hassani, 2003). Another advantage of employing a unit cell in FEA analysis is reducing the computational intensity of the FEA calculations (Johnston et al., 2006).

Several research studies on cellular structures applied FEA in order to compare or validate the experimental results. Harrysson et al. (2008) used ANSYS (ANSYS, Inc., Pennsylvania) to model cellular specimens with 3D beam elements in compression. It was found that the simulated elastic moduli were higher than the actual test results. Similarly, Consizoglu et al. (2008) also utilized ANSYS to simulate the compressive modulus and strength for cellular structures and compared them to the test results as the function of cell length and beam thickness for different cell sizes.

2.3 Chemical etching of Ti-6Al-4V

Etching, in general, can be explained as a controlled corrosion process occurring by electrolytic action at structural variations on the sample surface (Vander Voort, 1999). Chemical etching is done using etchants that are known to react with the metals being etched. These etchants typically consist of three main components known as corrosive agent, modifier and oxidizer. A modifier helps to reduce ionization while an oxidizer controls oxidation by absorbing electrons.

Several acids such as hydrochloric acid (HCl), sulfuric acid (H_2SO_4), hydrofluoric acid (HF) and nitric acid (HNO_3) are known to react with titanium. However, titanium and its alloys require strong etchants to remove the adherent oxide film on their surface, thus, a combination of HF and HNO_3 is commonly found in the etchants (Voort, 1999). However, proper ratios of both acids in the solution need to be selected carefully as it will affect the etching rate and the amount of hydrogen absorbed in cast Ti-6Al-4V (Wen and Yu, 2004). It was found that larger amounts of HNO_3 will reduce hydrogen absorption. Brunette et al., (2001) also suggested that the ratio of HF to HNO_3 need to be at 1:10 to reduce hydrogen absorption, as this will lead to surface embrittlement.

The effects of chemical etching on tissue ingrowth surfaces have been investigated in several studies. Dinda et al. (2008) used a Direct Metal Deposition process to fabricate Ti-6Al-4V scaffolds. These scaffolds' surface roughnesses were measured among untreated samples, sand-blasted samples, and sand-blasted and etched samples. The etching was done in 5 ml HF, 10ml HNO_3 and 85 ml H_2O for 5 minutes. The average roughness measured 25 μm, 12 μm and 8 μm respectively. Titanium discs were also built via EBM and human cell in-vitro studies were conducted (Springer, 2010). Some of the discs were etched with 2% HF, 30% HNO_3 and water for durations of 1 and 2 minutes. Cell viability tests showed that the numbers of living cell on the etched discs are greater than those on untreated ones. Surface roughnesses were reported to be around 22 μm, 15 μm and 12.5 μm for untreated, 1 minute etched and 2 minute etched discs respectively. Further investigation showed decreasing of strut sizes and increasing of pore diameters of the etched discs.

2.4 Problem Statement

This chapter has reviewed the manufacturing processes related to cellular structures. The flexibility of SFF technologies such as EBM has allowed more complex and refined structures to be built, and their properties tailored for specific applications. The mechanical behavior of non-stochastic structures has also been investigated and their applications, especially for implants and tissue ingrowth surfaces have been described. This research attempts to focus on the mechanical properties of small pore structures with different geometrical designs, in order to get better views on their similarities with human bones.

Several mesh structures with bigger pores were built in the initial stages of this research. It was found that the structures have a lot of powder trapped inside them even after an extensive cleaning process. The possibility of using the chemical etching process for removing the trapped powder will be studied along with its effects on mechanical and surface properties. The research also aims to gather initial understanding towards the fatigue characteristics of these periodic structures.

Chapter 3 Research Methodology

Cellular structures have been known to be used for numerous purposes, but it is important to mention that this research is conducted specifically for medical applications, especially implants. Two known issues associated with implants are tissue ingrowth and stress shielding. According to Harrysson et al. (2008), fixation strength of a cementless implant relies on its pore size. Tissues need certain surface conditions to grow on, and the same research has summarized that pore sizes between 50 μm to 800 μm are usually found to fulfill the requirement. Stress shielding is a situation where stress in some areas of the bone is reduced as some of the load is carried by the implant due to the mismatch in material properties between them, induced by the greater stiffness of the implant (Joshi et al., 2000). As a result, poor stress distribution occurs at the bone-implant interface which leads to bone resorption (Murr et al., 2010). The loss of bone mass from bone resorption can cause loosening of the prosthesis.

In order to overcome or reduce the significance of these problems, an implant having a good porous surface for tissue ingrowth while exhibiting mechanical properties similar to the bone needs to be used. This research addresses the problems by studying different cellular structures made by the EBM process with customized pore sizes and investigating their mechanical properties including compression and fatigue life at a specified stress.

Another aspect that this research will look into is the removing of the trapped powder. Chua et al. (2003) indicated that this is a common problem for powder based AM processes, especially when a thick part is made and the trapped powder is beyond reach. For this matter,

a chemical etching approach using hydrofluoric-nitric solution will be used and the process effects toward mechanical and structural properties will be observed.

The experiments are conducted based on two hypotheses, the samples without etching will show greater strength as they have more material, but the etched samples are supposed to have better fatigue life at a given stress as their surface conditions are better. A succinct summary of the experimental approach implemented for this research is as follows:

- Designing periodic structures with nominal pore size and strut size with SolidWorks (Dassault Systèmes SolidWorks Corp., Massachusetts) and Magics (Materialise, Belgium) softwares.
- Fabricating the mesh structures with the EBM process.
- Measuring the final pore and strut sizes with Hirox KH-7700 (Hirox-USA Inc., New Jersey) digital microscope.
- Statistical analysis to calculate the means and standard deviations for the measurements.
- Chemical etching of some of the samples with hydrofluoric-nitric acid solution.
- Measuring the new pore and strut sizes resulting from the etching process, and parting of samples for the observation of trapped powder.
- Conducting compressive and fatigue life testing.
- Evaluating the mechanical properties obtained from the tests.
- Building Finite Element Analysis models (FEA) based on the final structures and comparing the simulations results with the ones from the mechanical testing.

3.1 Design and fabrication of structures

Three different polyhedral structures were selected as the unit cells for the mesh structure fabrication in this research. They consist of hexagonal, rhombic dodecahedral and octahedral cell structures. Their unit cells were designed in SolidWorks with the characteristics shown in **Figure 15**. These unit cells were patterned to fill space and form a cube with the dimensions of approximately 25.4 x 25.4 x 25.4 mm. The struts were designed with a square profile rather than a circular one to reduce the size of the STL files. This will not be a problem as the thin EBM beam will produce an approximately circular strut cross section due to the melt pool. Due to SolidWorks limitations, most of the patterning procedures were carried out in the Magics software. After the unit cells were completely patterned, the STL files were fixed in the same software before being exported into the EBM A2 machine and sliced at 0.1 mm layer thickness with the software installed on the EBM (EBM Control 3.2).

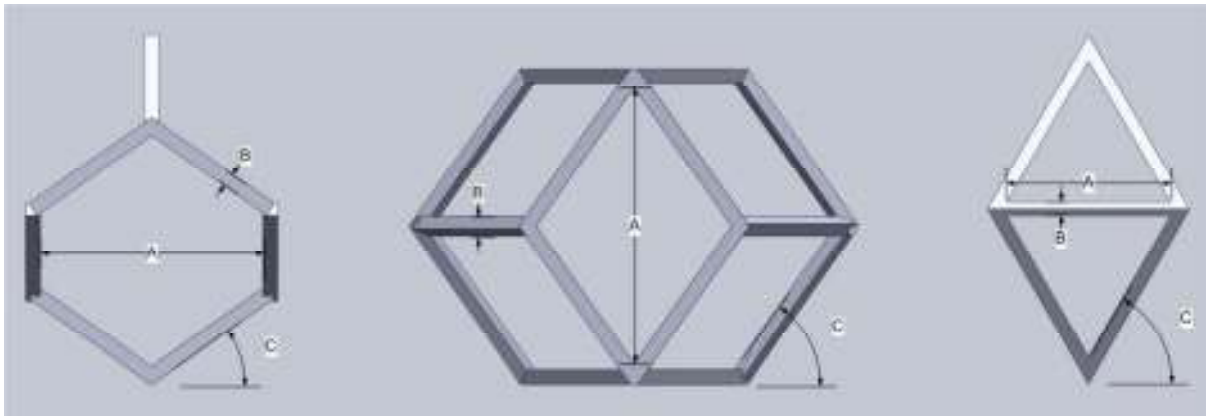

Figure 15 Unit cell characteristics for hexagonal, rhombic dodecahedral and octahedral: A is the pore size, B is the strut size and C is the build angle.

Before the first layer of Ti-6Al-4V powder was melted and the process proceeded as previously described, the build plate was preheated to 750˚C. The build chamber was cooled with Helium gas after the completion of each build. Parts were taken out of the chamber and cleaned with pressurized air containing titanium powder. In order to observe and compare the chemical etching effects toward removing the trapped powder in the later stage of this research, the cleaning time was set to 3 minutes for each cube, where each surface of the cube was cleaned for 30 seconds.

As previously mentioned in this chapter, the pore size of the structures needs to be below 800 μm to obtain good tissue ingrowth. To acquire the right pore size for these structures, they were built in smaller scales (**Figure 16**) and the resulting pores were measured using the Hirox KH-7700 digital microscope as shown in **Figure 17**. Based on this scaling method, it was found that the initial pore and strut values in **Table 3** produced pore sizes of approximately 600 μm. These initial values were used to build mesh specimens for the mechanical tests.

Table 3 Characteristics of unit cells used for the rest of the research.

Unit Cell Shape	Initial Pore size, mm	Initial Strut size, mm	Build angle
Hexagon	1.2	0.1	30˚
Rhombic Dodecahedron	1.5	0.1	54.74˚
Octahedron	1.4	0.1	53.13˚

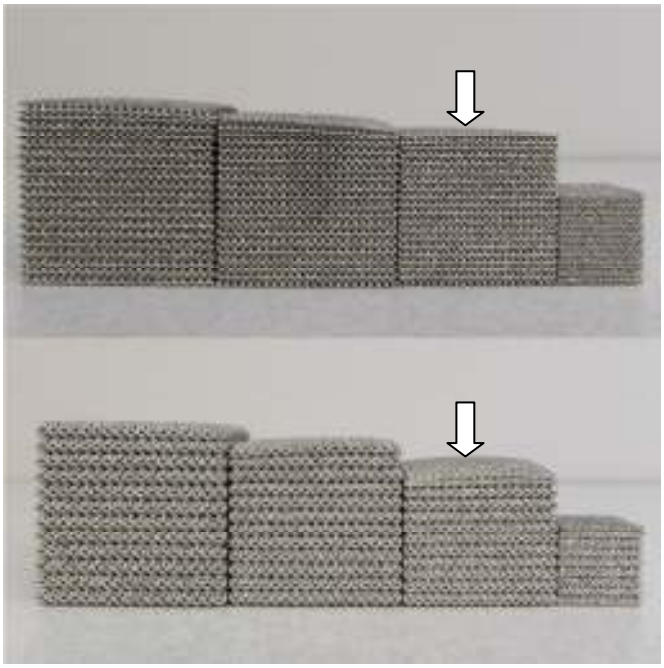

Figure 16 Scaling of structures. The ones on top are hexagonal, followed by rhombic dodecahedral. Structures used in this research are marked by the arrows in the picture.

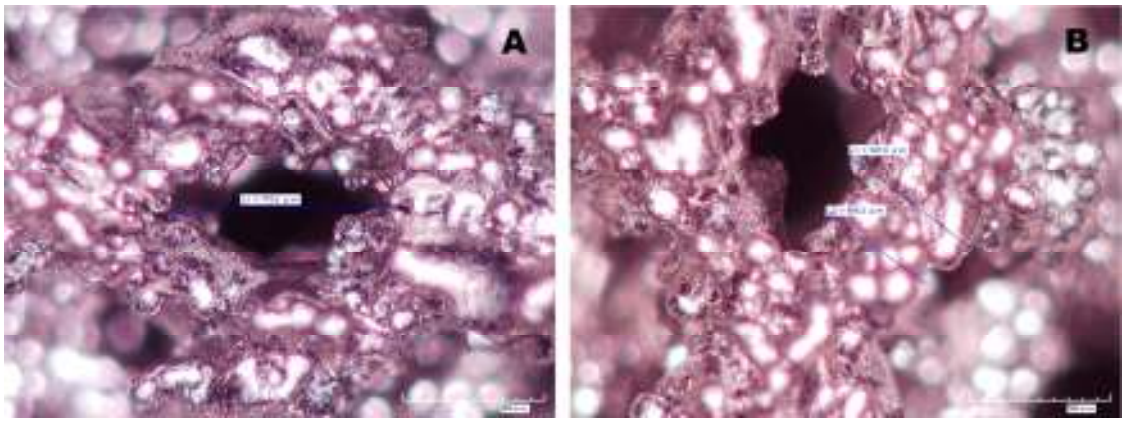

Figure 17 Pore measurement (A) and strut measurement (B) with Hirox KH-7700 digital microscope under 100X magnification.

3.2 Chemical etching procedure

A preliminary study was conducted to determine suitable etching conditions for this research. Twelve Ti-6Al-4V cubic mesh specimens were fabricated via EBM (four specimens for each cell shape) and the sizes were approximately 25.4 x 25.4 x 25.4 mm. Pre-etched relative densities for the hexagonal, rhombic dodecahedral and octahedral specimens were measured and the average values obtained were 0.33, 0.19 and 0.45, respectively. These specimens had larger pore sizes than the actual specimens used later in this research. Four groups consisting of three specimens, one from each cell shape, were formed and etched in hydrofluoric-nitric acid solution (2% HF, 20% HNO_3) under four different combinations of etchant volume and etching time; 200 ml for 90 seconds, 200 ml for 120 seconds, 400 ml for 90 seconds and 400 ml for 120 seconds. After each etching process, samples were rinsed inside a de-ionized water bath six times and dried with nitrogen. Post-etched relative densities were measured and compared to the pre-etched ones. The reductions of the relative densities are recorded as shown in **Figure 18** below:

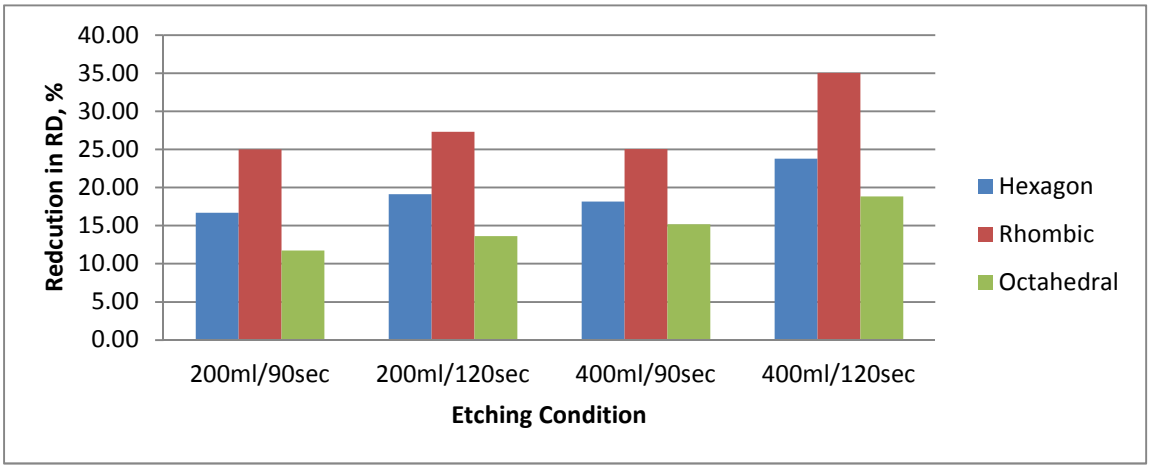

Figure 18 Average of percentage reduction in relative density for different etching conditions.

The results show that the etchant volume affects the material removal quantity when longer etching time is used. The corrosive agent in the etchant depleted over time and the etching rate will decrease. This effect was expected to become greater when actual specimens were used as they have more trapped powder due to their much smaller pore size. It can be seen that the first three conditions have similar results except for the octahedral. Based on this preliminary study, two etching conditions were selected for the mechanical tests; 400ml for 90 seconds and 400 ml for 120 seconds.

For the compression test, samples with the same dimension as the pilot study were fabricated while the specimens' sizes for the fatigue life testing were approximately 12.7 x 12.7 x 12.7 mm. In order to ensure that the smaller specimens have the same etching rate, lesser etchant volume was used. Three specimens were etched in 150 ml at a time in hydrofluoric-nitric acid solution for the same periods as specified above. **Table 4** below summarizes the number of specimens made and their allocations in this research:

Table 4 Allocation of samples for chemical etching and mechanical testing.

Mechanical Test	**Unit Cell Shape**	**Sample size, n**			**Total**
		Not etched	**90 sec**	**120 sec**	
Compression test (25.4 x 25.4 x 25.4 mm)	Hexagon	3	3	3	27
	Rhombic Dodecahedron	3	3	3	
	Octahedron	3	3	3	
Fatigue life test (12.7 x 12.7 x 12.7 mm)	Hexagon	2	2	2	17
	Rhombic Dodecahedron	1	2	2	
	Octahedron	2	2	2	
	Total	14	15	15	

3.3 Mechanical testing procedure

3.3.1 Compression test

This test was conducted on an ATS 1620-C universal tester and the size of specimens used was approximately 25.4 x 25.4 x 25.4 mm (**Figure 19**). Test samples were compressed between hardened steel plates connected to an extensometer. This extensometer was used to measure the displacement directly from the specimens rather than relying on the readings from the tester's crosshead. The test setup is shown in **Figure 20**. The compression rate was set at 1.27 mm/min and a total of 27 specimens were tested according to **Table 4**.

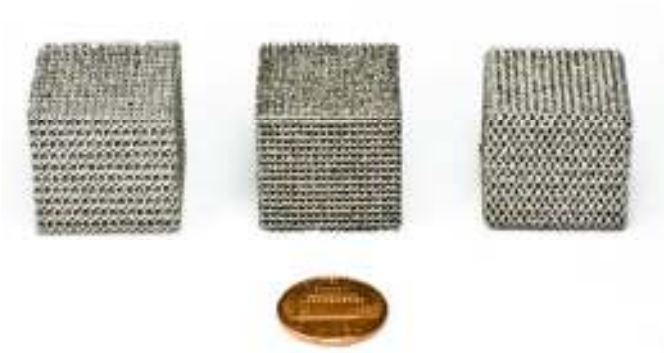

Figure 19 Specimens for compression testing.

Each specimen was compressed two times in the build direction (the Z-axis) as can be seen in **Figure 21**. The first test was intended to obtain the modulus of elasticity, thus, the specimen was compressed until a consistent linear elastic slope was observed on the stress-strain curve displayed on the monitor. After removing the extensometer, the test was restarted and the specimen was loaded until failure to record the actual peak load required for calculating the compressive strength. Visual observations of the structures' behavior throughout the test were recorded with a digital camera.

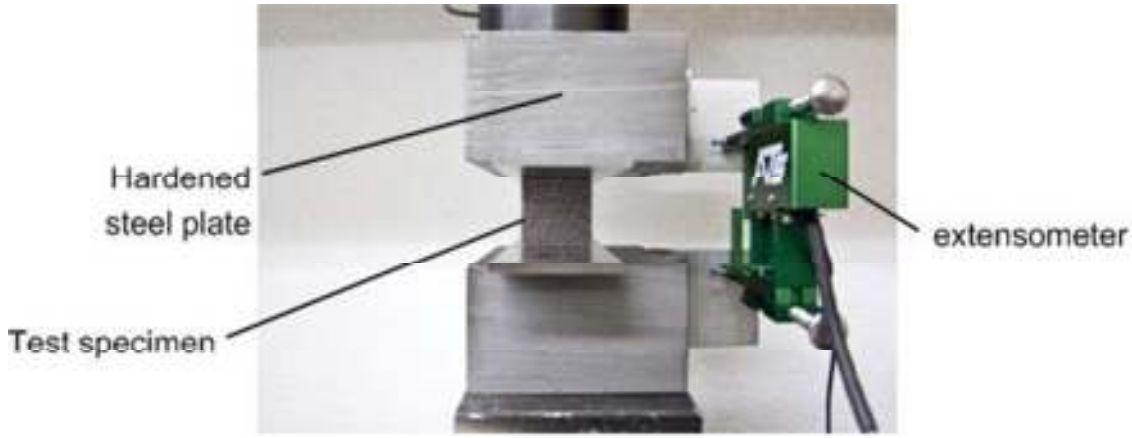

Figure 20 Compression test setup.

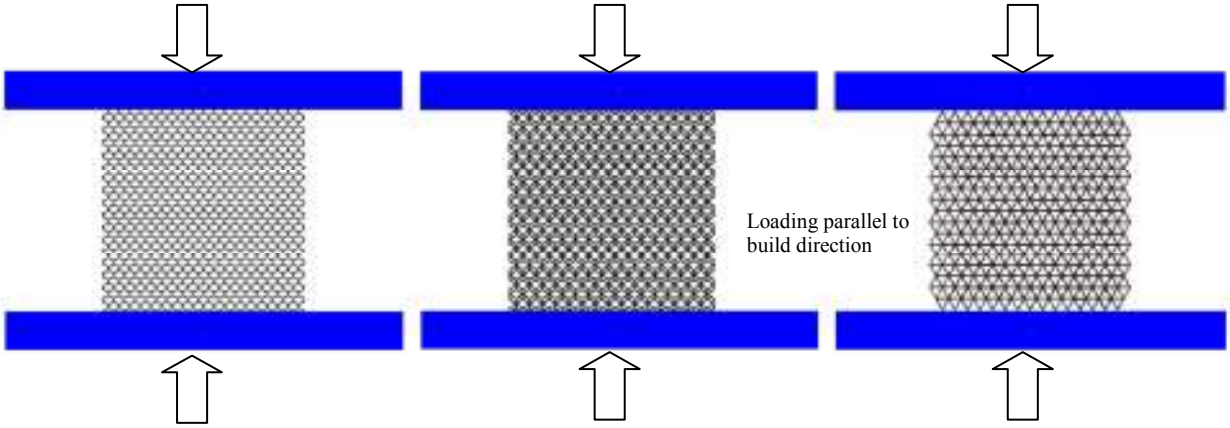

Figure 21 Compression was applied in the build direction of each sample. From left to right: hexagon, rhombic dodecahedron and octahedron specimens.

3.3.2 Fatigue life test

The size of the specimens used for the fatigue life testing was approximately 12.7 x 12.7 x 12.7, smaller than the test samples used for the compression testing (**Figure 22**). The reason behind this was that the equipment used for the fatigue test, TestResources 910LX3 System, has a much lower load limit than the universal testing machine used for the compression testing (3000 lb. vs. 20000 lb.). In total, 27 samples were tested as listed is

Table 4. The tests were conducted by applying cycles of alternating stress on the specimens parallel to its build direction. Applied load cycled between 25% and 2.5% of ultimate load, which gave a fatigue ratio value of 0.9. Loading frequency used was 10 Hz. The determination of the maximum compressive load was done by crushing one of the specimens. Failure of the structures occurred as they were subjected to repeated loading and unloading. The results obtained were the numbers of cycles to failure, which is known as fatigue life, N_f. The testing apparatus for the fatigue life is shown in **Figure 23**.

Figure 22 Specimens for fatigue testing.

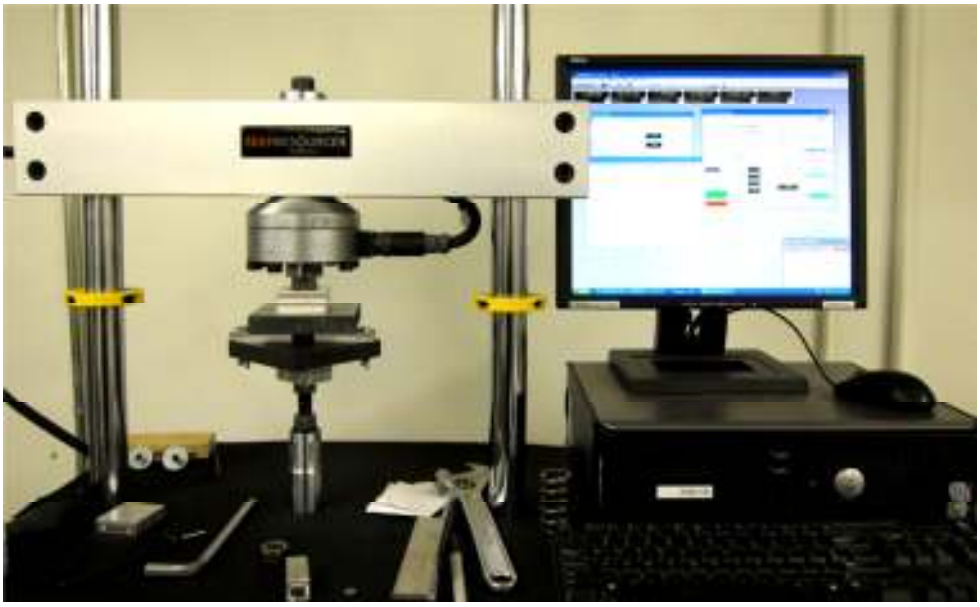

Figure 23 Fatigue test conducted on TestResources 910LX3 Desktop System.

3.4 Trapped powder estimation

Nine samples were used to evaluate the effect of chemical etching toward reducing the amount of trapped powder inside the mesh, 3 samples for each cell shape, which consist of un-etched, 90 seconds etching and 120 seconds etching. Sample size used was exactly the same as the sample size for compression testing. Each cube was mounted in low viscosity resin and parted into two sections parallel to the build direction with a water cooled SiC abrasive cut-off saw after the resin was cured.

During the mounting process, the plastic cup containing the resin melt and the cube was placed in a chamber connected to a vacuum pump to increase the penetration of resin into the mesh. Next, the parting surface was polished to obtain an optimal surface condition for microscopic inspection. The amount of trapped powder was measured in terms of surface area as the region with and without powder inside the mesh can be differentiated

distinctively. The surfaces were also inspected under Hirox KH-7700 digital microscope. **Figure 24** below shows the cross-sectional area of a parted hexagon cube.

Figure 24 Cross sections of a hexagon cube showing the trapped powder inside.

Chapter 4 Results and Discussion

4.1 Measurements of structures

Twenty seven parts were measured in terms of their strut and pore sizes. Twelve readings were taken from each specimen, three from each surface parallel to the build direction (4 surfaces in total). The top and bottom surface of the cubes were not measured because they have different cell layouts. **Table 5** and **Table 6** list the measurement results of struts and pores respectively, measured with the Hirox KH-7700 digital microscope. The values presented below are the averages of three specimens.

Table 5 Strut sizes of lattice structures in different etching conditions.

Structure	Etching Condition	Average Strut Diameter (μm)	Standard Deviation
Hexagonal	not etched	515.13	40.32
	90 seconds	376.02	33.81
	120 seconds	302.30	23.40
Rhombic Dodecahedral	not etched	478.28	31.77
	90 seconds	300.84	35.03
	120 seconds	253.80	22.08
Octahedral	not etched	467.70	36.43
	90 seconds	357.09	31.47
	120 seconds	311.14	23.28

Table 6 Pore sizes of lattice structures in different etching conditions.

Structure	Etching Condition	Average Pore Size(μm)	Standard Deviation
Hexagonal	not etched	572.41	48.08
	90 seconds	726.65	61.14
	120 seconds	864.03	50.81
Rhombic Dodecahedral	not etched	603.96	56.59
	90 seconds	907.95	67.90
	120 seconds	1057.02	73.43
Octahedral	not etched	601.88	57.26
	90 seconds	843.31	75.85
	120 seconds	951.48	59.84

4.2 Compression tests

Samples were labeled with the letters H, R and O for hexagonal, rhombic dodecahedral and octahedral, respectively. The samples were also numbered from 1 to 9, where samples 1 to 3 were not etched, samples 4 to 6 were etched for 90 seconds and samples 7 to 9 were etched for 120 seconds. **Figure 25** shows the compression test results for the nine hexagonal specimens. These specimens were compressed in a direction parallel to the build direction as described in the previous chapter. It can be seen from the data that the unetched samples were stronger and stiffer, followed by the 90 seconds etched and 120 seconds etched specimens. The same trend was also observed for the etched and unetched parts of rhombic dodecahedral and octahedral structures as shown in **Figure 26** and **Figure**

27. Detailed results including relative density and average of modulus and strength are given in **Table 7**. Ultimate load values used to calculate the compressive strength were taken from the onset of failure. The values of coefficient of variation in **Table 7** indicate that the compressive strengths of etched samples have wider distributions compared to the unetched specimens.

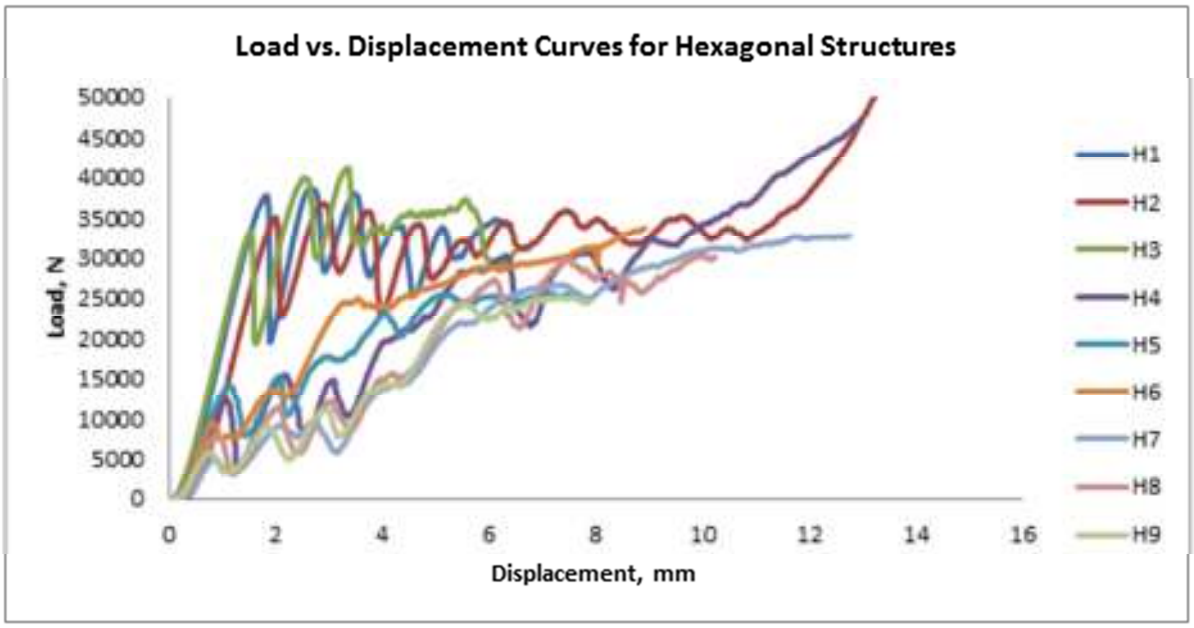

Figure 25 Compression test results for hexagonal structures.

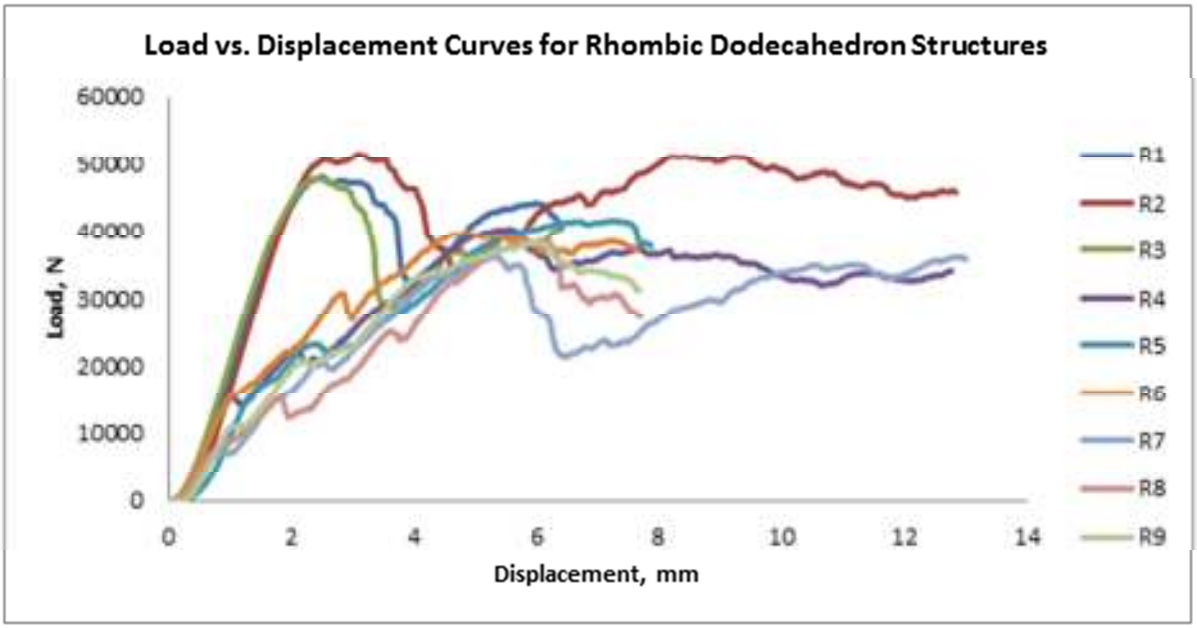

Figure 26 Compression test results for rhombic dodecahedral structures.

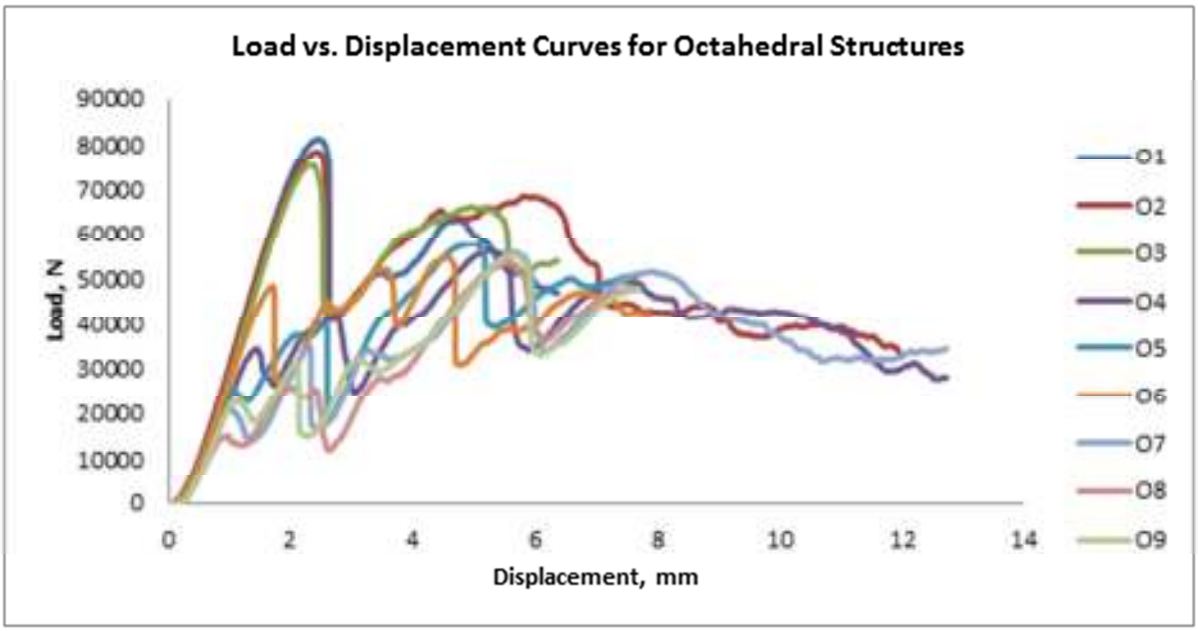

Figure 27 Compression test results for octahedral structures.

Table 7 Summary of compression test results for all structures.

Sample #	Relative Density	Elastic Modulus, MPa	Compressive Strength, MPa	Average Modulus, MPa, with coefficient of variation	Average Strength, MPa, with coefficient of variation
R1	0.3548	2068	68.56	2056.67 (0.0392)	69.54 (0.0364)
R2	0.3708	1971	72.42		
R3	0.3557	2131	67.65		
R4	0.3173	1327	22.42	1196.67 (0.1149)	33.57 (0.3318)
R5	0.2985	1210	33.60		
R6	0.3158	1053	44.70		
R7	0.3103	826	10.40	839.00 (0.0535)	16.08 (0.3402)
R8	0.2840	802	21.94		
R9	0.2922	889	15.89		
H1	0.3498	1765	54.40	1663.33 (0.0538)	51.88 (0.0665)
H2	0.3528	1628	53.31		
H3	0.3723	1597	47.94		
H4	0.3350	889	18.08	910.67 (0.0348)	17.56 (0.2005)
H5	0.3104	896	20.79		
H6	0.3198	947	13.81		
H7	0.3057	508	7.13	526.00 (0.0375)	9.13 (0.2618)
H8	0.2547	523	11.78		
H9	0.2817	547	8.49		
O1	0.4031	3062	118.09	3140.33 (0.0378)	113.54 (0.0419)
O2	0.4203	3277	113.91		
O3	0.4091	3082	108.60		
O4	0.3387	2335	50.14	2352.00 (0.0673)	52.73 (0.3211)
O5	0.3632	2518	37.24		
O6	0.3256	2203	70.81		
O7	0.3090	1613	30.12	1676.67 (0.0345)	28.48 (0.2001)
O8	0.3338	1691	22.14		
O9	0.3117	1726	33.17		

The corrosive action from the chemical etching processes clearly reduced the mass of the structures, hence decreasing their relative densities. **Figure 28** and **Figure 29** below show the changes in elastic modulus and compressive strength of the parts at different levels of

relative density obtained via etching. The values used in both figures are the average values calculated from **Table 7** above.

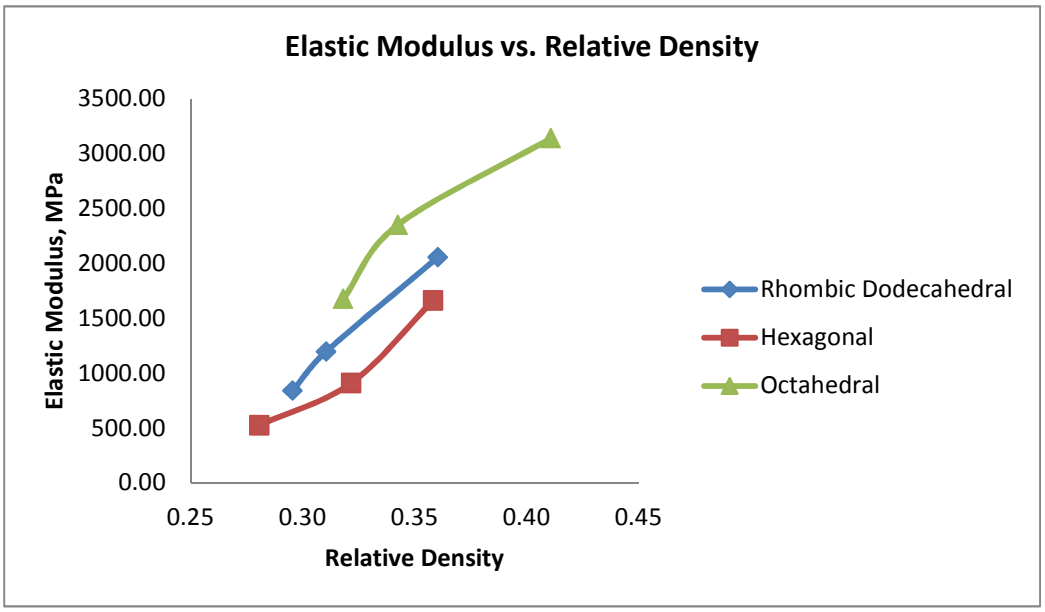

Figure 28 Comparison of elastic modulus among structures as a function of relative density.

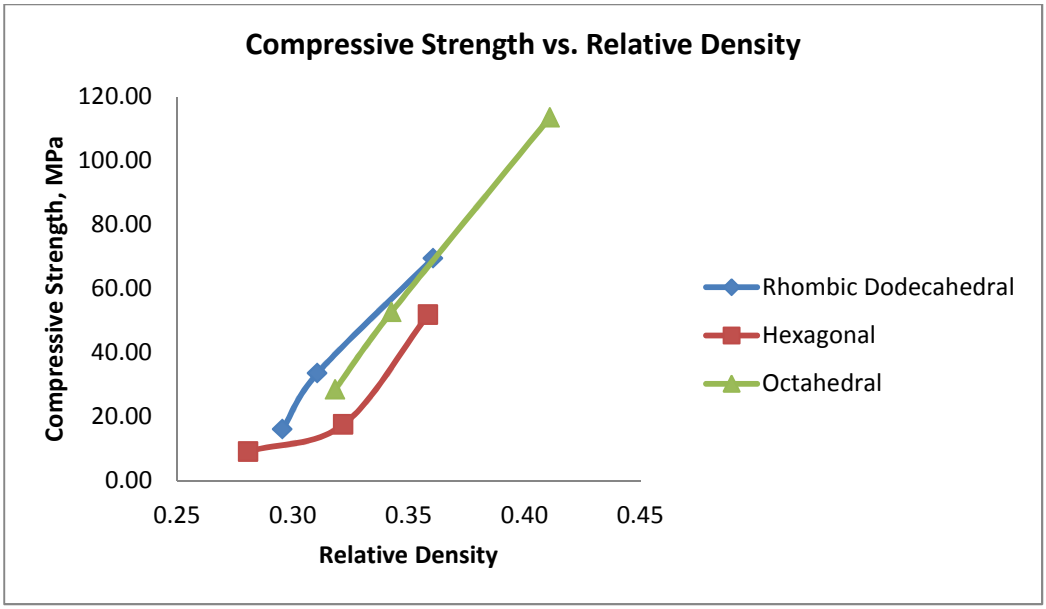

Figure 29 Comparison of compressive strength among structures as a function of relative density.

4.2.1 Finite Element Analysis (FEA)

COSMOSWorks (Dassault Systèmes SolidWorks Corp., Massachusetts) was used for the Finite Element Analysis of the lattice structures. A single unit cell of each cell geometry was analyzed using the boundary conditions shown in **Figure 30** below. Other input parameters were Poisson's Ratio = 0.3 and Elastic Modulus, E = 110 GPa, which are the standard values for titanium.

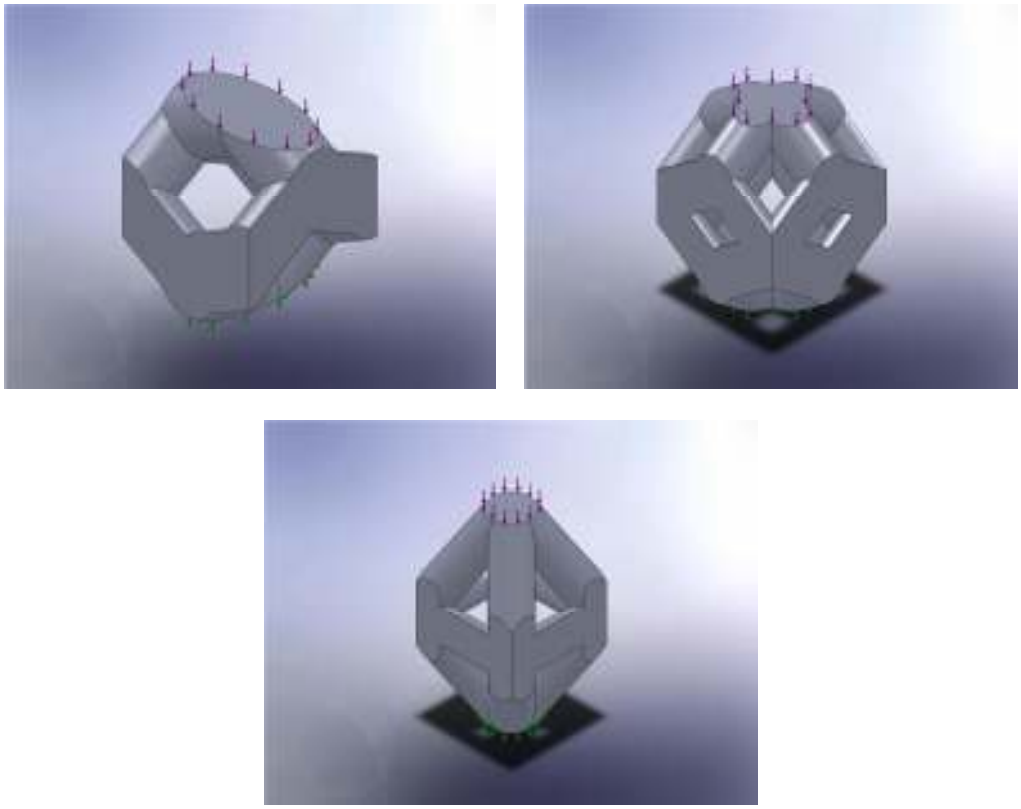

Figure 30 Boundary conditions of the unit cells for FEA; (1) hexagonal unit cell, (2) rhombic dodecahedral unit cell and (3) octahedral unit cell.

The results in **Figure 31** clearly show that the elastic modules values obtain from the FEA are higher than the experimental ones. This is expected as the models used in FEA are design with circular struts and have no defects. Data obtained from compression testing

showed that the rhombic dodecahedral structures are slightly stiffer than the hexagonal structures, but the FEA results indicated the opposite.

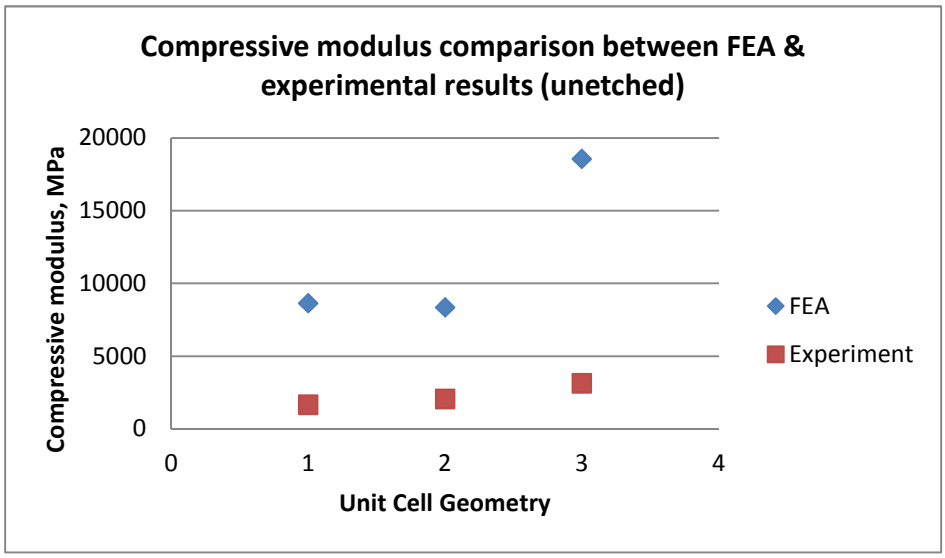

Figure 31 Comparison of compressive modulus values obtained from FEA and experiment for unetched samples. Unit cell 1 is a hexagonal, 2 is a rhombic dodecahedral and 3 is an octahedral.

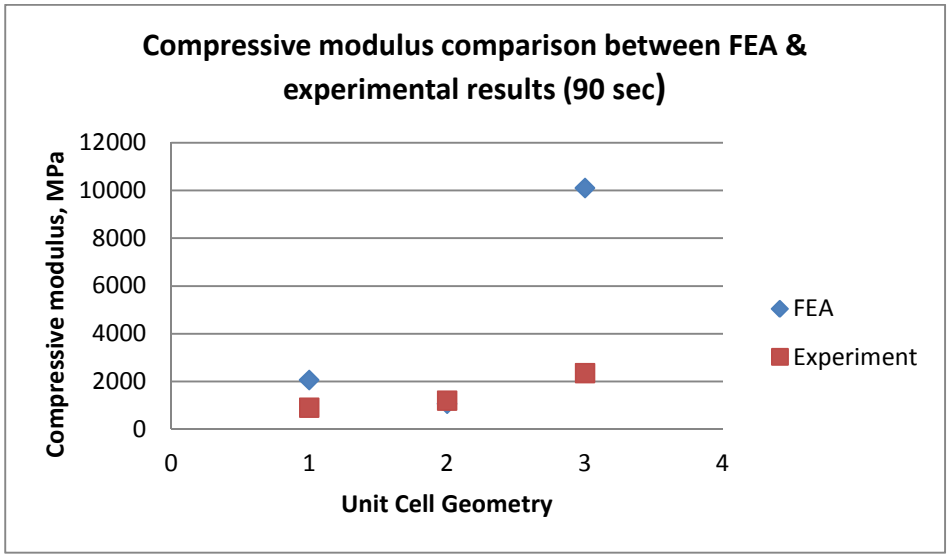

Figure 32 Comparison of compressive modulus values obtained from FEA and experiment for 90 seconds etched samples. Unit cell 1 is a hexagonal, 2 is a rhombic dodecahedral and 3 is an octahedral.

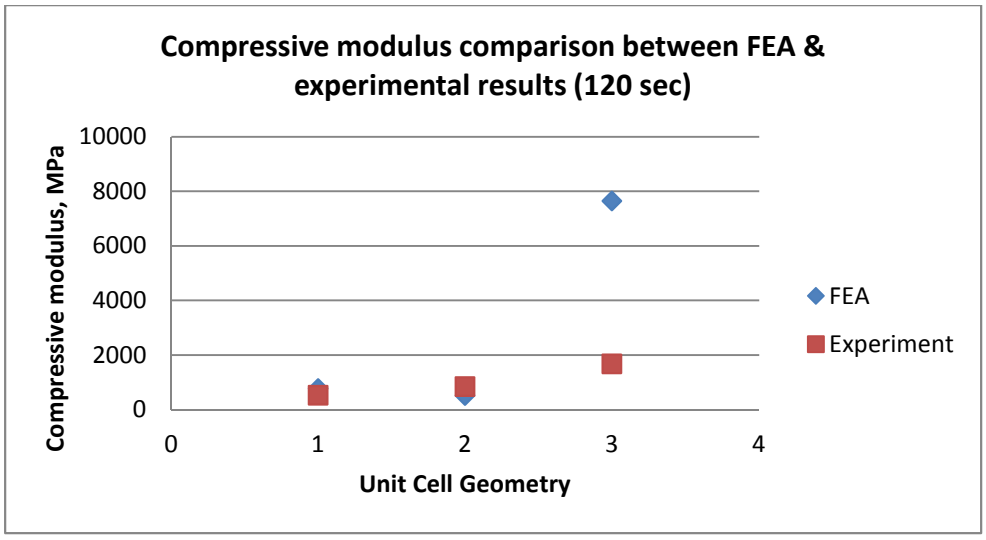

Figure 33 Comparison of compressive modulus values obtained from FEA and experiment for 120 seconds etched samples. Unit cell 1 is a hexagonal, 2 is a rhombic dodecahedral and 3 is an octahedral.

Figure 32 and **Figure 33** indicate that the differences between the FEA results and the experimental data are smaller for etched hexagonal and rhombic dodecahedral, but remain large for octahedral. This is caused by the missing or defected horizontal struts on the octahedral structures, which made them much weaker and harder to predict. FEA results for octahedral structures without the horizontal struts show the same trend as the other structures as shown in **Figure 34** below.

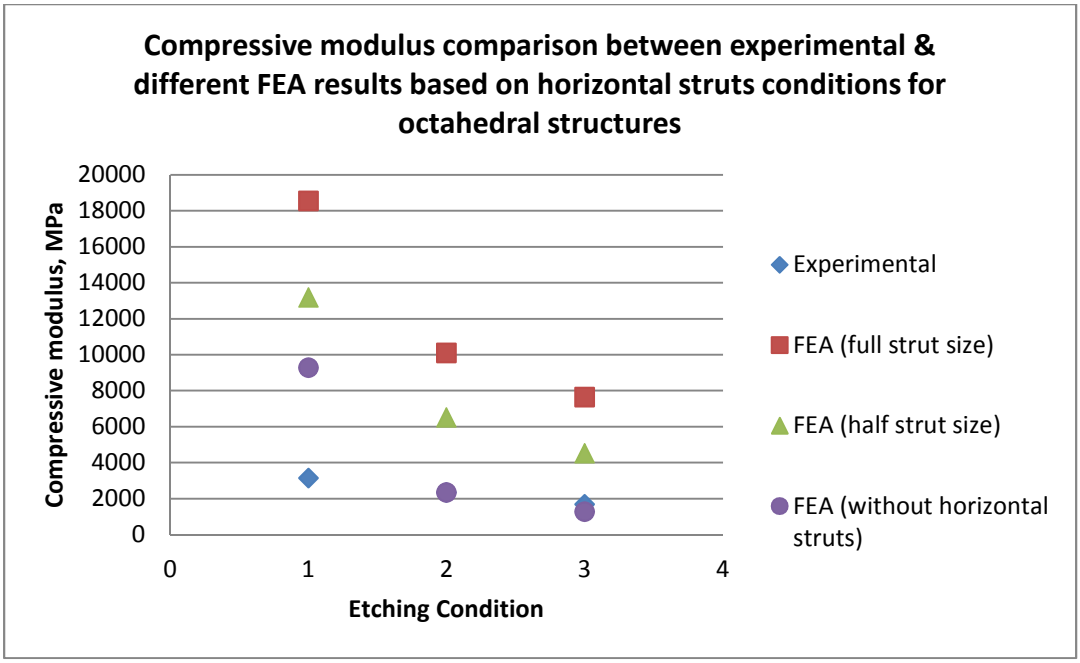

Figure 34 Experimental and FEA results for compressive modulus of octahedral structures with different horizontal strut sizes in different etching conditions; (1) unetched, (2) 90 seconds etched, and (3) 120 seconds etched.

4.3 Fatigue life tests

The fatigue lives observed show distinctive differences between the etched and un-etched samples as depicted in **Figure 35**, **Figure 36** and **Figure 37**. In general, etched structures yielded higher cycle to failure, which supports the second hypothesis of the study. However, the variability, especially between the etched samples, is very large. Differences in a factor of 10 were observed between 2 samples etched with the exact same parameters, except for the 120 seconds etched rhombic dodecahedral specimens. The one with higher fatigue life did not fail after 5 million cycles and the test was stopped as this value is considered high enough. One possible explanation for this condition is that the samples were fabricated in 3 different builds. This could cause inconsistencies in build conditions. In

addition, some defects (voids) were observed on the samples which might be exaggerated by the etching process.

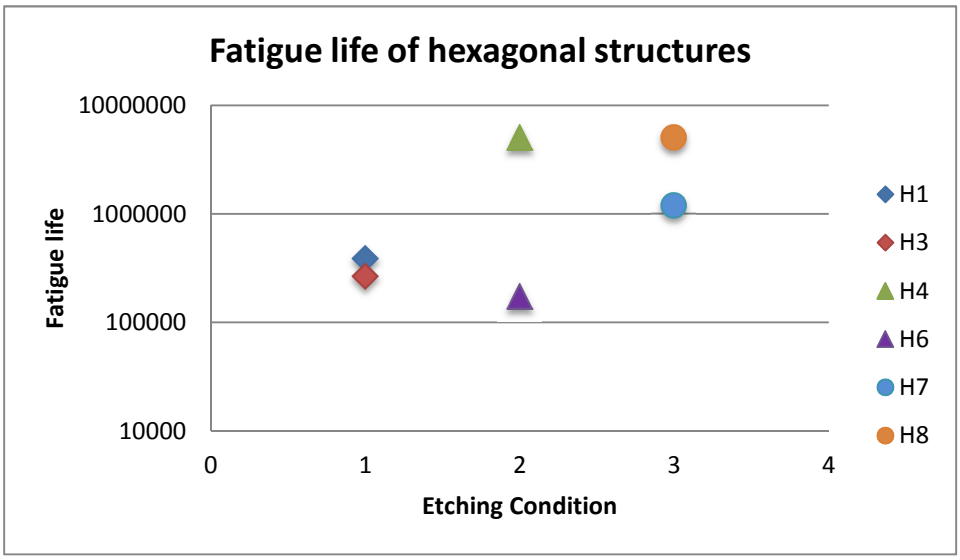

Figure 35 Fatigue lives of hexagonal structures on different etching conditions; (1) un-etched, (2) 90 seconds etched and (3) 120 seconds etched.

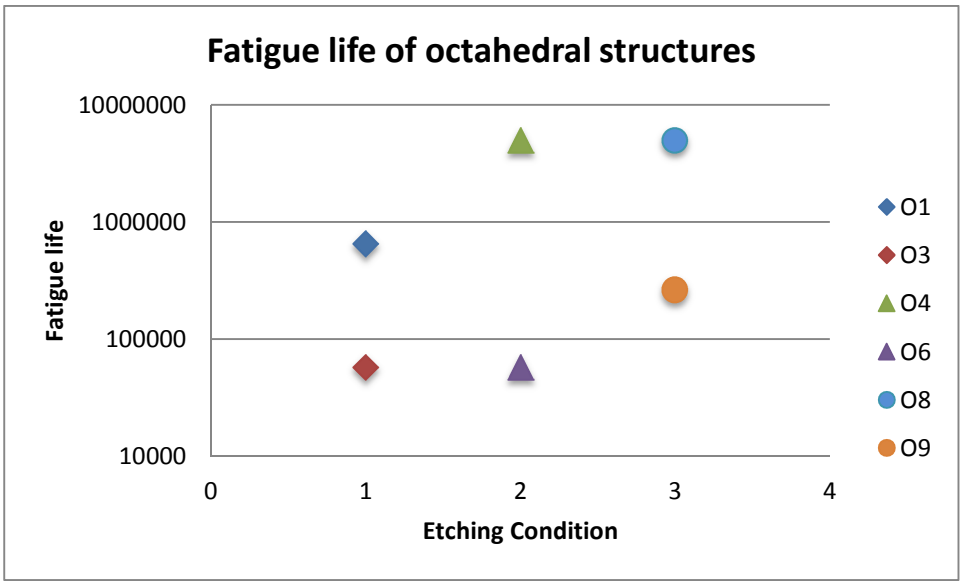

Figure 36 Fatigue lives of octahedral structures on different etching conditions; (1) un-etched, (2) 90 seconds etched and (3) 120 seconds etched.

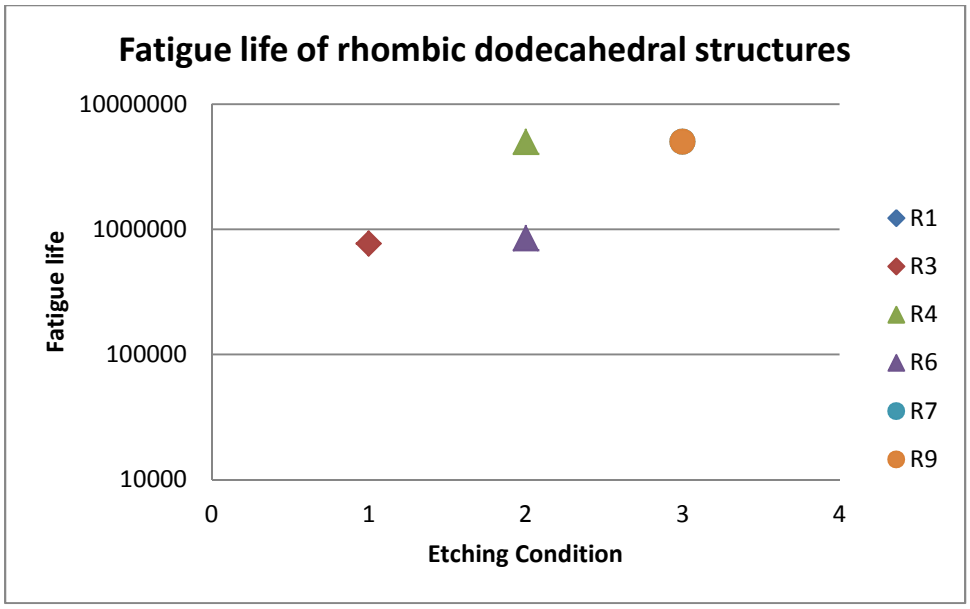

Figure 37 Fatigue lives of rhombic dodecahedral structures on different etching conditions; (1) un-etched, (2) 90 seconds etched and (3) 120 seconds etched.

4.4 Trapped powder removal

Trapped powder within the mesh structures was measured by calculating the area possessed by the powder each cube's cross section as shown is **Figure 38**. A standard measuring ruler was used as it was not possible to obtain the entire image of the cross-section with the Hirox KH-7700 digital microscope even with the smallest magnification. Furthermore, the areas occupied by the powder are approximately rectangular in shape, so measuring their edges was not difficult. **Table 8** below lists out the outcomes of the evaluation.

Figure 38 Cross sections of hexagon cubes showing the trapped powder inside the mesh structures. From left to right: not etched, 90 seconds etched and 120 seconds etched.

Table 8 Measured area of trapped powder inside the cellular structures.

Unit Cell	Etching Condition	Area of trapped powder (mm^2)
Hexagonal	Not etched	298.06
	90 sec	316.13
	120 sec	297.29
Rhombic Dodecahedral	Not etched	243.87
	90 sec	245.68
	120 sec	260.13
Octahedral	Not etched	261.93
	90 sec	270.97
	120 sec	254.45

4.5 Discussion

The results above show that the mechanical properties of chemically etched Ti-6Al-4V lattice structures fabricated via EBM vary significantly from the un-etched ones. They possessed lower compressive modulus and strength, and this can be explained by the lesser

amount of material that they have in the struts leading to lower relative densities, which agree with the first hypothesis of this research. The results also indicate that the variations in the compressive strength of the etched specimens are greater, even though they were etched with the same conditions, which can be seen from **Table 7**. These variations might have been caused by exaggerated flaws in the structures by the chemical etching process.

Failure mode during compression testing was observed and the difference between un-etched and etched samples was noticed. The samples without etching typically failed at a certain load due to macroscopic shearing as shown in **Figure 39**. These shear cracks occurred along the plane with the angles approximately the same as the build angles listed in **Table 3**. The etched samples also produced similar shear cracks, but these were not their initial cause of failure during testing. They collapsed gradually, where the top and bottom layers were crushed and the cracks were initiated on a later stage as depicted in **Figure 40**.

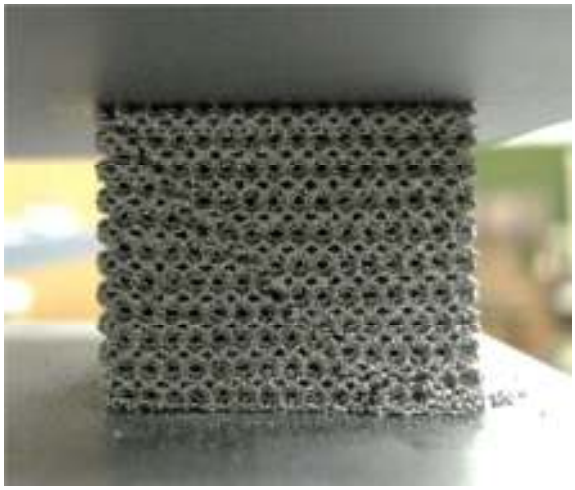

Figure 39 Failure of the un-etched rhombic dodecahedral lattice structure.

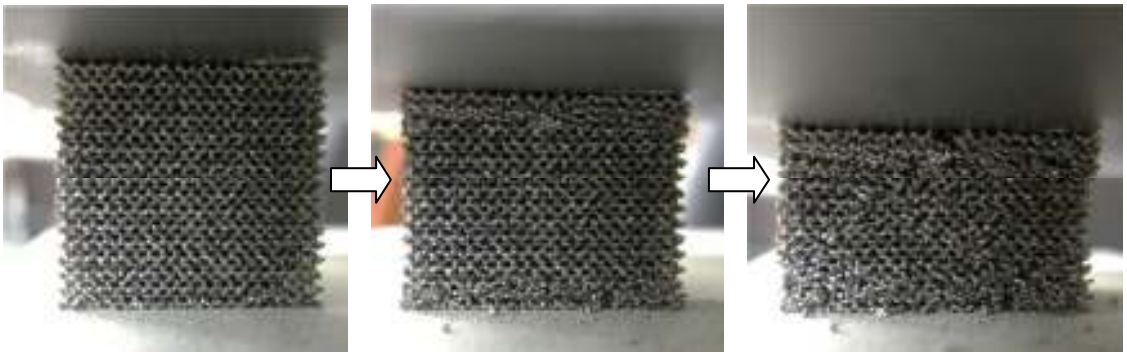

Figure 40 Collapse mode of etched hexagonal structure.

While the etched samples were reduced in weight, relative density and strut size, no significant changes in trapped powder were observed from the samples' cross sections. Further inspection under Hirox KH-7700 digital microscope clearly showed the region with and without powder as shown in **Figure 41**. The dark area on the right side of each figure is powder free, but there were no other indications to differentiate between the un-etched and etched structures. It is not clear whether the decrease in weight was contributed only by the strut sizes reduction or along with trapped powder removal. Results from **Table 8** also indicate that the hexagonal structures have the most powder trapped in every condition. This is consistent with their pore sizes which are relatively smaller compared to rhombic dodecahedral and octahedral structures.

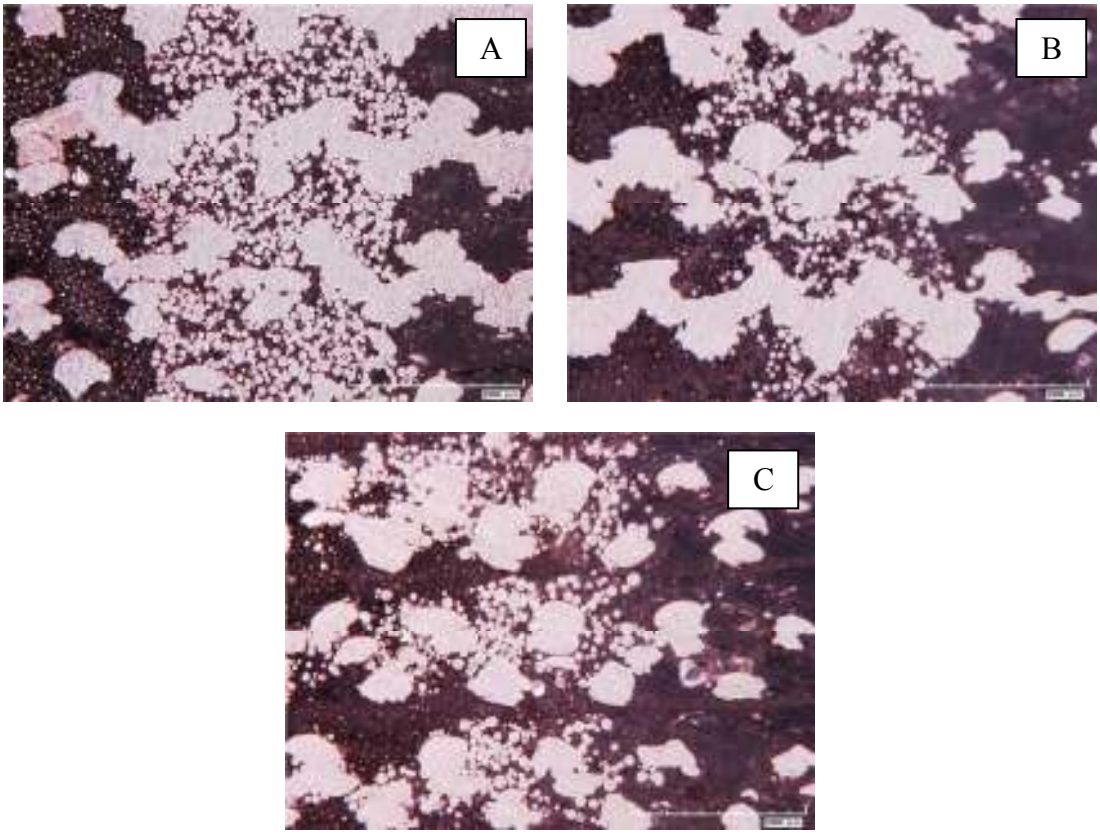

Figure 41 Microscopic observations from the cross section of un-etched (A), 90 seconds etched (B) and 120 seconds etched (C) hexagonal cubes with Hirox KH-7700 digital microscope under 50X magnification.

Chapter 5 Conclusions and Recommendations

5.1 Conclusions

In this study, the mechanical properties such as elastic modulus, compressive strength and fatigue life of three different cell geometries (hexagonal, rhombic dodecahedral and octahedral) under three different conditions, without etching, etched for 90 seconds and etched for 120 seconds with hydrofluoric-nitric acid solution were investigated and compared along with their relative densities. The aforementioned mesh structures were only tested parallel to the build direction (the z-direction).

In general, the octahedral structures showed the highest value of elastic modulus and compressive strength, while the structures with hexagonal cells gave the lowest value. In terms of relative density, octahedral cubes also possessed the highest readings. There were only slight differences on relative density between the hexagonal and rhombic dodecahedral lattice structures. The chemical etching process clearly reduced the mass of the structures which can be seen through the changes in strut and pore sizes, and also the decrease in relative density. Mass reduction leads to weaker structures in compression testing which supports the first hypothesis of this study.

Significantly higher fatigue lives were observed for etched specimens, but the relationship between etching time and fatigue life could not be established due to small sample sizes. A better approach would be to select one specific cell geometry and simultaneously build all samples of the structure to eliminate slight differences due to process variability. Chemical etching was also used as an approach to remove the trapped

powder inside the lattice structures. However, there was no significant effect observed from the cross-sections of the mounted cubes.

5.2 Recommendations for future study

- Due to the time constraint, this study only covered the compression properties and compressive fatigue life of the cellular structures. However, implants such as hip stems are also subjected to bending stress. For future experiments, it is suggested that the flexural and the bending fatigue characteristics of these structures be investigated.

- It was observed that parts from different EBM builds vary significantly in fatigue life under the same amount of load. For future research, parts should be fabricated in a single build to obtain more precise and accurate data.

- Other approaches to remove trapped powder within the lattice structures should be explored. Chemical etching did not show any visible effect in reducing the trapped powder. Suggested methods are ultrasonic bath and mechanical vibrations via vibrating plate. Another approach is to directly etch the specimens without blasting them first.

- Developing the S-N curve will be useful to obtain information regarding the fatigue behaviour of the cellular structures.

- Recently, Arcam has introduced EBM Multibeam^{tm} technology which resulted in faster scanning speed and finer surface characteristics. This development has

given an opportunity to fabricate more refined structures with smaller pore sizes for further studies their mechanical properties.

REFERENCES

Ashby M.F., Evans A., Fleck N.A., Gibson L.J., Hutchinson J.W. and Wadley H.N.G. (2000), *Metal Foams A Design Guide*, Elsevier.

Ashby M.F. (2006), "The properties of foams and lattices", *Philosophical Transactions of the Royal Society A*, 364, 15-30.

Banhart J. (2000), "Manufacturing Routes for Metallic Foams", *Journal of the Minerals, Metals and Materials Society*, 52(12), 22-27.

Banhart J. and Weaire D. (2002), "On the road again: metal foams find favor", *Physics Today*, 55, 37-42.

Bertol L.S., W.K. Junior, F.P. da Silva and C. Aumund-Kopp (2010), "Medical design: Direct metal laser sintering of Ti-6Al-4V", *Materials and Design*, 31, 3982-3988.

Brunette D., P. Tengvall, M. Textor and P. Thomsen (2001), *Titanium in Medicine: Material Science, Surface Science, Engineering, Biological Response and Medical Applications*, Springer.

Calladine C.R. (1983), *Theory of shell structures*, Cambridge University Press.

Cansizoglu O., (2008), "Mesh Structures with Tailored Properties and Applications in Hip Stem", *PhD Dissertation*, North Carolina State University, Raleigh.

Cansizoglu O., O. Harrysson, D. Cormier, H. West and T. Mahale (2008), "Properties of Ti-6Al-4V non-stochastic lattice structures fabricated via electron beam melting", *Materials Science and Engineering A*, 492, 468-474.

Chen C., T.J. Lu and N.A. Fleck (1999), "Effect of imperfections on the yielding of two-dimensional foams", *Journal of the Mechanics and Physics of Solids*, 47, 2235-2272.

Chua C.K., K.F. Leong, C.M. Cheah and S.W. Chua (2003), "Development of a Tissue Engineering Scaffold Structure Library for Rapid Prototyping. Part 1: Investigation and Classification", *The International Journal of Advanced Manufacturing Technology*, 21, 291-301.

Chu C.L., C.Y. Chung, P.H. Lin and S.D. Wang (2004), "Fabrication of porous NiTi shape memory alloy for hard tissue implants by combustion synthesis", *Materials Science and Engineering A*, 366, 114-119.

Cormier D., H. West, O. Harrysson and K. Knowlson (2004), "Characterization of thin walled Ti-6Al-4V components produced via electron beam melting", *Proceedings of SFF 2004*.

Davies G.J., S. Zhen (1983), "Metallic foams: their production, properties and applications", *Journal of Material Science*, 18, 1899-1911.

Dinda G.P., L. Song and J. Mazumder (2008), "Fabrication of Ti-6Al-4V Scaffolds by Direct Metal Deposition", *Metallurgical and Materials Transactions A*, 39, 2914-2922.

Espana F.A., V.K. Balla, S. Bose and A. Bandyopadhyay (2010), "Design and fabrication of CoCrMo alloy based novel structures for load bearing implants using laser engineered net shaping", *Materials Science and Engineering C*, 30, 50-57.

Gibson L.J. (2000), "Mechanical Behavior of Metallic Foams", *Annual Review of Materials Science*, 30, 191-227.

Gibson L.J. and Ashby M.F. (1997), *Cellular solids: structure & properties*, second ed., Cambridge University Press.

Grenestedt J.L. (2005), "On interactions between imperfections in cellular solids", *Journal of Materials Science*, 40, 5853-5857.

Harrysson O.L.A., O. Cansizoglu, D.J. Marcellin-Little (2009), "Comparison of direct metal fabrication technologies for production of medical implants", *Proceedings of RAPID 2009*.

Harrysson O.L.A., O. Cansizoglu, D.J. Marcellin-Little, D.R. Cormier and H.A. West II (2008), "Direct metal fabrication of titanium implants with tailored materials and mechanical properties using electron beam melting technology", *Materials Science and Engineering C*, 28, 366-373.

Hollander D.A., Matthias von Walter, T. Wirtz, R. Sellei, B. Schmidt-Rohlfing, O. Paar and Hans-Josef Erli (2006), " Structural, mechanical and in vitro characterization of invidually structured Ti-6Al-4V produced by direct laser forming", *Biomaterials*, 27, 955-963.

Johnston S.R., D.W. Rosen, M. Reed and H.V. Wang (2006), "Analysis if Mesostructure Unit Cells Comprised of Octet-truss Structures", *Proceedings of SFF 2006*.

Joshi M.G., S.G. Advani, F. Miller and M.H. Santare (2000), "Analysis if a femoral hip prosthesis designed to reduce stress shielding", Journal of Biomechanics, 33, 1655-1662.

Kim H.S. and Al-Hassani S.T.S. (2003), "Effective elastic constants of two-dimensional cellular materials with deep and thick cell walls", *International Journal of Mechanical Sciences, 45, 1999-2016*.

Kumar V. (2009), "Effect of Shape and Density on Electrical Conductivity of Non-Stochastic Lattice Structure", *MS Thesis*, North Carolina State University, Raleigh.

Kusakabe H., T. Sakamaki, K. Nihei, Y. Oyama, S. Yanagimoto, M. Ichimiya, J. Kimura and Y. Toyama (2004), "Osseointegration of a hydroxyapatite-coated multilayered mesh stem", *Biomaterials*, 25, 2957-2969.

Li J.P., J.R. de Wijn, C.A.V. Blitterswijk and K. de Groot (2006), "Porous Ti_6Al_4V scaffold directly fabricating by rapid prototyping: Preparation and in vitro experiment", *Biomaterials*, 27, 1223-1235.

Manogharan G.P. (2009), "Analysis of Non-Stochastic Lattice Structure Design for Heat Exchanger Application", *MS Thesis*, North Carolina State University, Raleigh.

Queheillalt D.T. and H.N.G Wadley (2005), "Cellular metal lattices with hollow trusses", *Acta Materialia*, 53, 303-313.

Murr L.E., S.M. Gaytan, F. Medina, H. Lopez, E. Martinez, B.I. Machado, D.H. Hernandez, L. Martinez, M.I. Lopez, R.B. Wicker and J. Bracke (2010), "Next-generation biomedical implants using additive manufacturing of complex, cellular and functional mesh arrays", Philosophical Transactions of The Royal Society A, 368, 1999-2032.

Murr L.E., S.M. Gaytan, F. Medina, M.I. Lopez, E. Martinez and R.B. Wicker (2009), "Additive layered manufacturing of reticulated Ti-6Al-4V by Electron Beam Melting", *IFMBE Proceedings*, 24, 23-28.

Queheillalt D.T. and H.N.G Wadley (2009), "Titanium alloy lattice truss structures", *Materials and Design*, 30, 1966-1975.

Rabiei A. and Vendra L.J. (2009), "A comparison of composite metal foam's properties and other comparable metal foams", *Material Letters*, 63, 533-536.

Ryan G., A. Pandit, and D.P. Apatsidis (2006), "Fabrication methods of porous metals for use in orthopaedic applications", *Biomaterials*, 27, 2651-2670.

Springer J.S. (2010), "In vitro Studies of Titanium Alloy Discs Fabricated with Electron Beam Melting for Improving Transdermal Osseointegrated Implant Surfaces", *PhD Dissertation*, North Carolina State University, Raleigh.

Vander Voort G.F. (1999), *Metallography Principles and Practice*, ASM International.

Wadley H.N.G. (2002), "Cellular metals manufacturing", *Advanced Engineering Materials*, 4(10), 726-733.

Wadley H.N.G. (2006), "Multifunctional periodic cellular metals", *Philosophical Transactions of the Royal Society A*, 364, 31-68.

Wadley H.N.G., N.A. Fleck and A.G. Evans (2003), "Fabrication and structural performance of periodic cellular metal sandwich structures", *Composites Science and Technology*, 63, 2331-2343.